Acta Mechanica Solida Sinica 30 (2017) 209–222

Available online at www.sciencedirect.com

ScienceDirect

journal homepage: www.elsevier.com/locate/CAMSS

Nonlinear buckling and postbuckling behavior of cylindrical shear deformable nanoshells subjected to radial compression including surface free energy effects

S. Sahmani, M.M. Aghdam, M. Bahrami*

Department of Mechanical Engineering, Amirkabir University of Technology, P.O. Box 15875-4413, Tehran, Iran

ARTICLE INFO

Article history:
Received 31 August 2015
Accepted 26 December 2015
Available online 13 February

Keywords:
Nanoscale structures
Size effect
Nonlinear buckling
Surface free energy
Boundary layer theory

ABSTRACT

The objective of the present investigation is to predict the nonlinear buckling and postbuckling characteristics of cylindrical shear deformable nanoshells with and without initial imperfection under hydrostatic pressure load in the presence of surface free energy effects. To this end, Gurtin-Murdoch elasticity theory is implemented into the first-order shear deformation shell theory to develop a size-dependent shell model which has an excellent capability to take surface free energy effects into account. A linear variation through the shell thickness is assumed for the normal stress component of the bulk to satisfy the equilibrium conditions on the surfaces of nanoshell. On the basis of variational approach and using von Karman-Donnell-type of kinematic nonlinearity, the non-classical governing differential equations are derived. Then a boundary layer theory of shell buckling is employed incorporating the effects of surface free energy in conjunction with nonlinear prebuckling deformations, large deflections in the postbuckling domain and initial geometric imperfection. Finally, an efficient solution methodology based on a two-stepped singular perturbation technique is put into use in order to obtain the critical buckling loads and postbuckling equilibrium paths corresponding to various geometric parameters. It is demonstrated that the surface free energy effects cause increases in both the critical buckling pressure and critical end-shortening of a nanoshell made of silicon.

1. Introduction

Several application potentials of nanotechnology that appeared for a short to medium-term time range could lead to significant improvements within several areas of space technology. Nanoengineering could produce surfaces that regulate spacecraft temperatures more efficiently than the materials used today. It could also generate more efficient solar cells, rendering large panels redundant.

Therefore, nanostructures such as ultra thin plates (nanofilms), nanobeams, nanoshells, etc. have attracted much attention from the scientific community due to their considerably enormous physical, mechanical, and electrical properties [1–3]. Across the applications, when the thickness of the general structures reaches the order of submicron size, the size-dependent influence of material plays an essential role in the mechanical behavior of nanostructures. The classical continuum models are independent of the

* Corresponding author. Fax: +98 21 66419736.
E-mail address: aghdam@aut.ac.ir (M.M. Aghdam).

http://dx.doi.org/10.1016/j.camss.2017.02.002
0894-9166/

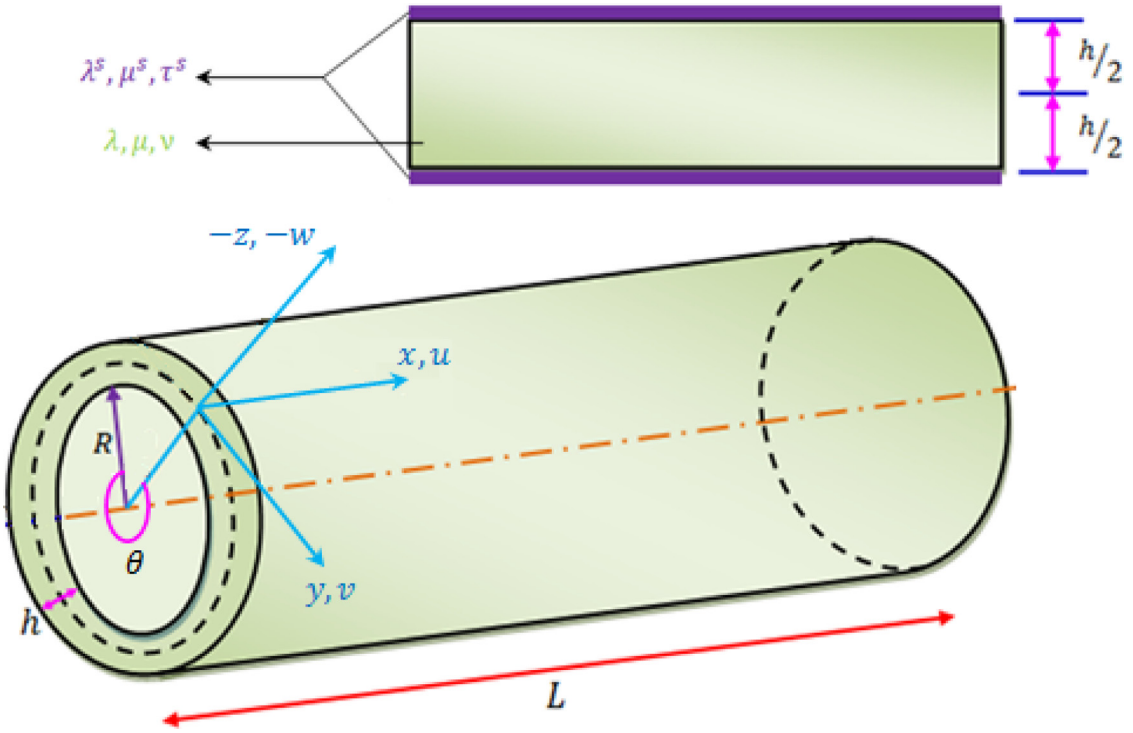

Fig. 1 – Schematic view of a cylindrical shear deformable nanoshell with surface layers.

scale of structures, making it controversial to implement them in nanomaterials for small scale effect. As reported in several studies, the length scales associated with material microstructures are often small enough to call the capability of the classical continuum models into question. Hence, to extend the continuum mechanics to accommodate the size dependence of microstructures becomes a topic of major concern. Modified continuum models are among the most applied theoretical approaches for the investigation of nanomechanics due to their computational efficiency and capability of producing accurate results which are comparable to those from the atomistic models [4–23].

Surface stress effect is one of these effects. The high surfacetobulk ratio causes nanostructures to behave differently compared with conventional structures. Gurtin and Murdoch [24,25] developed a theoretical framework based on continuum mechanics including surface stress effects, in which the surface was simulated as a mathematical layer of zero thickness with different material properties from the underlying bulk which was completely bonded by the membrane. They presented the following general and simple expression for the surface stress-strain relation

$$\sigma^s_{ij} = \tau_s\delta_{ij} + (\tau_s + \lambda_s)\varepsilon_{kk}\delta_{ij} + 2(\mu_s - \tau_s)\varepsilon_{ij} + \tau_s u^s_{i,j} \ (i, j = x, y)$$
$$\sigma^s_{iz} = \tau_s u^s_{z,i} \qquad (1)$$

where λ_s and μ_s are the surface Lame constants, and τ_s denotes the residual surface stress under unstrained conditions.

It should be noted that the surface elastic constants are quite different from the bulk elastic constants as the former have dimensions of N/m, which are different from the latter with dimensions of N/m^2. It has been shown that the surface can be assumed to behave isotropically, and it is still meaningful to use appropriate average of surface stress [25-27].

The Gurtin-Murdoch model has the capability of incorporating the effects of surface free energy into the mechanical response of nanostrustures efficiently. This fact has been examined in several studies conducted for different problems about the mechanical behavior of structures at nanoscale [28-52].

In the current study, a non-classical shell model is introduced in order to predict the effects of surface free energy on the nonlinear buckling and postbuckling behavior of cylindrical shear deformable nanoshells subjected to radial compressive load. For this purpose, novel size-dependent differential equations are derived on the basis of Gurtin-Murdoch elasticity theory in conjunction with the first-order shear deformation shell theory. Afterwards, the size-dependent governing differential equations are converted into the boundary layer-type equations. Subsequently, a two-stepped singular perturbation technique is utilized to obtain the size-dependent critical buckling pressures and the postbuckling equilibrium paths for nanoshells with different geometric parameters.

2. Mathematical formulations

As shown in Fig. 1, a cylindrical shear-deformable nanoshell with length L, thickness h, and mid-surface radius R is considered. The nanoshell includes a bulk part and two additional thin surface layers (the inner and outer layers). For the bulk part, the material properties are Young's modulus E and Poisson's ratio ν. The two surface layers are assumed to have

surface elasticity modulus E_s, Poisson's ratio ν_s and residual surface tension τ_s. According to a curvilinear coordinate system with its origin located on the middle surface of nanoshell, coordinates of a typical point in the axial, circumferential and radial directions are denoted by x, y and z, respectively. Now, in accordance with the classical shell theory, the displacement field can be expressed as

$$u_x(x,y,z) = u(x,y) + z\psi_x(x,y) \tag{2a}$$

$$u_y(x,y,z) = v(x,y) + z\psi_y(x,y) \tag{2b}$$

$$u_z(x,y,z) = w(x,y) \tag{2c}$$

in which u, v and w denote the middle surface displacements along the x, y and z axis, respectively, and ψ_x and ψ_y are respectively the rotations of middle surface normals about the y- and x- axis.

Based upon the von Karman-Donnell-type kinematics of nonlinearity [53], it is assumed that the thickness of the shell, h, is remarkably small in comparison with its radius of curvature R, and the kinematical strain-displacement relationship can be given as follows

$$\begin{Bmatrix}\varepsilon_{xx}\\ \varepsilon_{yy}\\ \gamma_{xy}\end{Bmatrix} = \begin{Bmatrix}\varepsilon^0_{xx}\\ \varepsilon^0_{yy}\\ \gamma^0_{xy}\end{Bmatrix} + z\begin{Bmatrix}\kappa_{xx}\\ \kappa_{yy}\\ \kappa_{xy}\end{Bmatrix} = \begin{Bmatrix}\frac{\partial u}{\partial x} + \frac{1}{2}\left(\frac{\partial w}{\partial x}\right)^2 + \frac{\partial w}{\partial x}\frac{\partial w^*}{\partial x}\\ \frac{\partial v}{\partial y} - \frac{w+w^*}{R} + \frac{1}{2}\left(\frac{\partial w}{\partial y}\right)^2 + \frac{\partial w}{\partial y}\frac{\partial w^*}{\partial y}\\ \frac{\partial u}{\partial y} + \frac{\partial v}{\partial x} + \frac{\partial w}{\partial x}\frac{\partial w}{\partial y} + \frac{\partial w}{\partial x}\frac{\partial w^*}{\partial y} + \frac{\partial w}{\partial y}\frac{\partial w^*}{\partial x}\end{Bmatrix} + z\begin{Bmatrix}\frac{\partial \psi_x}{\partial x}\\ \frac{\partial \psi_y}{\partial y}\\ \frac{\partial \psi_x}{\partial y} + \frac{\partial \psi_y}{\partial x}\end{Bmatrix} \tag{3a}$$

$$\begin{Bmatrix}\gamma_{xz}\\ \gamma_{yz}\end{Bmatrix} = \begin{Bmatrix}\psi_x + \frac{\partial w}{\partial x}\\ \psi_y + \frac{\partial w}{\partial y}\end{Bmatrix} \tag{3b}$$

where $\varepsilon^0_{xx}, \varepsilon^0_{xx}, \gamma^0_{xy}$ are the strain components of the middle surface, κ_{xx}, κ_{yy}, κ_{xy} denote the curvature components of nanoshell, and w^* stands for the initial geometric imperfection.

Afterwards, the constitutive relations can be written as

$$\begin{Bmatrix}\sigma_{xx}\\ \sigma_{yy}\\ \sigma_{xy}\\ \sigma_{xz}\\ \sigma_{yz}\end{Bmatrix} = \begin{bmatrix}\lambda+2\mu & \lambda & 0 & 0 & 0\\ \lambda & \lambda+2\mu & 0 & 0 & 0\\ 0 & 0 & \mu & 0 & 0\\ 0 & 0 & 0 & \mu & 0\\ 0 & 0 & 0 & 0 & \mu\end{bmatrix}\begin{Bmatrix}\varepsilon_{xx}\\ \varepsilon_{yy}\\ \gamma_{xy}\\ \gamma_{xz}\\ \gamma_{yz}\end{Bmatrix} \tag{4}$$

in which $\Lambda = (E^*\nu)/((1+\nu)(1-2^*\nu))$ and $\mu = E/(2(1+\nu))$ are Lame constants.

The classical concepts of continuum mechanics are incapable of considering the atomic features of nanostructures. However, for simplicity and computational efficiency of continuum mechanics, different modified continuum models have been developed to incorporate size-effects into the conventional continuum approach. In the present work, the modified continuum elasticity based on Gurtin-Murdoch theory is utilized to develop a size-dependent shell model for nonlinear buckling and postbuckling analysis of nanoshells in the presence of surface free energy effects. On the basis of equation (1), the components of surface stress can be determined with respect to the displacement components as follow

$$\begin{aligned}
\sigma^s_{xx} &= (\lambda_s + 2\mu_s)\varepsilon_{xx} + (\tau_s + \lambda_s)\varepsilon_{yy} + \tau_s - \frac{\tau_s}{2}\left(\frac{\partial(w+w^*)}{\partial x}\right)^2\\
\sigma^s_{yy} &= (\lambda_s + 2\mu_s)\varepsilon_{yy} + (\tau_s + \lambda_s)\varepsilon_{xx} + \frac{\tau_s}{R}(w+w^*)\\
&\quad + \tau_s - \frac{\tau_s}{2}\left(\frac{\partial(w+w^*)}{\partial y}\right)^2\\
\sigma^s_{xy} &= \mu_s\gamma_{xy} - \tau_s\left(\frac{\partial v}{\partial x} + \frac{\partial(w+w^*)}{\partial x}\frac{\partial(w+w^*)}{\partial y} + z\frac{\partial \psi_y}{\partial x}\right)\\
\sigma^s_{yx} &= \mu_s\gamma_{xy} - \tau_s\left(\frac{\partial u}{\partial y} + \frac{\partial(w+w^*)}{\partial x}\frac{\partial(w+w^*)}{\partial y} + z\frac{\partial \psi_x}{\partial y}\right)\\
\sigma^s_{xz} &= \tau_s\frac{\partial w}{\partial x}, \quad \sigma^s_{yz} = \tau_s\frac{\partial w}{\partial y}
\end{aligned} \tag{5}$$

In the classical shell theories, because the stress component σ_{zz} is small in comparison with other components of stress, it is assumed that $\sigma_{zz} = 0$. But this assumption does not satisfy the surface conditions related to the Gurtin-Murdoch model. To solve this problem, it is assumed that the stress component σ_{zz} varies linearly through the shell thickness and satisfies the balance conditions on the surfaces [39]. According to this assumption, σ_{zz} can be obtained as

$$\sigma_{zz} = \frac{\left(\frac{\partial\sigma^{S+}_{xz}}{\partial x} + \frac{\partial\sigma^{S+}_{yz}}{\partial y}\right) - \left(\frac{\partial\sigma^{S-}_{xz}}{\partial x} + \frac{\partial\sigma^{S-}_{yz}}{\partial y}\right)}{2} + \frac{\left(\frac{\partial\sigma^{S+}_{xz}}{\partial x} + \frac{\partial\sigma^{S+}_{yz}}{\partial y}\right) + \left(\frac{\partial\sigma^{S-}_{xz}}{\partial x} + \frac{\partial\sigma^{S-}_{yz}}{\partial y}\right)}{h}z \tag{6}$$

in which the superscripts S^+ and S^- refer to the inner and outer surfaces of nanoshell, respectively. Through inserting equation (5) into equation (6), σ_{zz} can be achieved as follows

$$\sigma_{zz} = \frac{2\tau_s z}{h}\left(\frac{\partial^2 w}{\partial x^2} + \frac{\partial^2 w}{\partial y^2}\right) \tag{7}$$

As a result, by substituting σ_{zz} into the constitutive equation (3) corresponding to the normal stresses (σ_{xx}, σ_{yy}) for the bulk of the nanoshell, one will have

$$\sigma_{xx} = (\lambda + 2\mu)\varepsilon_{xx} + \lambda\varepsilon_{yy} + \frac{\nu\sigma_{zz}}{(1-\nu)} \tag{8a}$$

$$\sigma_{yy} = (\lambda + 2\mu)\varepsilon_{yy} + \lambda\varepsilon_{xx} + \frac{\nu\sigma_{zz}}{(1-\nu)} \tag{8b}$$

Based on the continuum surface elasticity theory, the total strain energy of a cylindrical shear-deformable nanoshell in the presence of surface stress effects can be expressed as

$$\begin{aligned}
\Pi_s &= \frac{1}{2}\int_S\int_{-\frac{h}{2}}^{\frac{h}{2}}\sigma_{ij}\varepsilon_{ij}\mathrm{d}z\mathrm{d}S + \frac{1}{2}\left(\int_{S^+}\sigma^s_{ij}\varepsilon_{ij}\mathrm{d}S^+ + \int_{S^-}\sigma^s_{ij}\varepsilon_{ij}\mathrm{d}S^-\right)\\
&= \frac{1}{2}\int_S\Big\{\bar{N}_{xx}\varepsilon^0_{xx} + \bar{N}_{yy}\varepsilon^0_{yy} + \bar{N}_{xy}\gamma^0_{xy} + \bar{M}_{xx}\kappa_{xx} + \bar{M}_{yy}\kappa_{yy}\\
&\quad + \bar{M}_{xy}\kappa_{xy} + Q_x\gamma_{xz} + Q_y\gamma_{yz} + Q^s_x\frac{\partial w}{\partial x} + Q^s_y\frac{\partial w}{\partial y}\Big\}\mathrm{d}S
\end{aligned} \tag{9}$$

where S is the area occupied by the middle surface of the nanoshell. In equation (9), the resultants including in-plane

forces, bending moments and shear forces can be expressed as

$$\bar{N}_{xx} = N_{xx} + \sigma_{xx}^{s+} + \sigma_{xx}^{s-} = A_{11}^{*}\varepsilon_{xx}^{0} + A_{12}^{*}\varepsilon_{yy}^{0} + 2\tau_s - \tau_s\left(\frac{\partial(w+w^*)}{\partial x}\right)^2$$

$$\bar{N}_{yy} = N_{yy} + \sigma_{yy}^{s+} + \sigma_{yy}^{s-} = A_{11}^{*}\varepsilon_{yy}^{0} + A_{12}^{*}\varepsilon_{xx}^{0} + \frac{2\tau_s}{R}(w+w^*) + 2\tau_s - \tau_s\left(\frac{\partial(w+w^*)}{\partial y}\right)^2$$

$$\bar{N}_{xy} = N_{xy} + \frac{1}{2}\left(\sigma_{xy}^{s+} + \sigma_{yx}^{s+} + \sigma_{xy}^{s-} + \sigma_{yx}^{s-}\right) = A_{55}^{*}\gamma_{xy}^{0} - \tau_s\frac{\partial(w+w^*)}{\partial x}\frac{\partial(w+w^*)}{\partial y}$$

$$\bar{M}_{xx} = M_{xx} + \frac{h}{2}(\sigma_{xx}^{s+} - \sigma_{xx}^{s-}) = D_{11}^{*}\kappa_{xx} + D_{12}^{*}\kappa_{yy} + E_{11}^{*}\left(\frac{\partial^2 w}{\partial x^2} + \frac{\partial^2 w}{\partial y^2}\right)$$

$$\bar{M}_{yy} = M_{yy} + \frac{h}{2}\left(\sigma_{yy}^{s+} - \sigma_{yy}^{s-}\right) = D_{11}^{*}\kappa_{yy} + D_{12}^{*}\kappa_{xx} + E_{11}^{*}\left(\frac{\partial^2 w}{\partial x^2} + \frac{\partial^2 w}{\partial y^2}\right)$$

$$\bar{M}_{xy} = M_{xy} + \frac{h}{4}\left(\sigma_{xy}^{s+} + \sigma_{yx}^{s+} - \sigma_{xy}^{s-} - \sigma_{yx}^{s-}\right) = D_{55}^{*}\kappa_{xy}$$

$$Q_x = k_s A_{55}^{*}\gamma_{xz}, \quad Q_y = k_s A_{55}^{*}\gamma_{yz}$$

$$Q_x^s = \sigma_{xz}^{s-} + \sigma_{xz}^{s+} = 2\tau_s\frac{\partial w}{\partial x}, \quad Q_y^s = \sigma_{yz}^{s-} + \sigma_{yz}^{s+} = 2\tau_s\frac{\partial w}{\partial y} \tag{10}$$

in which k_s represents shear correction factor, and

$$\begin{Bmatrix} N_{xx} \\ N_{yy} \\ N_{xy} \end{Bmatrix} = \int_{-\frac{h}{2}}^{\frac{h}{2}} \begin{Bmatrix} \sigma_{xx} \\ \sigma_{yy} \\ \sigma_{xy} \end{Bmatrix} dz, \quad \begin{Bmatrix} M_{xx} \\ M_{yy} \\ M_{xy} \end{Bmatrix} = \int_{-\frac{h}{2}}^{\frac{h}{2}} \begin{Bmatrix} \sigma_{xx} \\ \sigma_{yy} \\ \sigma_{xy} \end{Bmatrix} z dz,$$

$$\begin{Bmatrix} Q_x \\ Q_y \end{Bmatrix} = k_s \int_{-\frac{h}{2}}^{\frac{h}{2}} \begin{Bmatrix} \sigma_{xz} \\ \sigma_{yz} \end{Bmatrix} dz \tag{11}$$

and

$$A_{11}^{*} = (\lambda + 2\mu)h + 2(\lambda_s + 2\mu_s), \quad A_{12}^{*} = \lambda h + 2\tau_s + 2\lambda_s,$$

$$A_{55}^{*} = \mu h + 2\mu_s - \tau_s \; D_{11}^{*} = \frac{(\lambda+2\mu)h^3}{12} + \frac{(\lambda_s+2\mu_s)h^2}{2},$$

$$D_{12}^{*} = \frac{\lambda h^3}{12} + \frac{(\tau_s+\lambda_s)h^2}{2}, \quad E_{11}^{*} = \frac{\nu h^2 \tau_s}{6(1-\nu)},$$

$$D_{55}^{*} = \frac{\mu h^3}{12} + \frac{(2\mu_s - \tau_s)h^2}{4} \tag{12}$$

Moreover, the work Π_P done by the external radial load, q can be expressed in the following form

$$\Pi_P = \int_S q w dS \tag{13}$$

Now, by using the below virtual work's principle

$$\delta\int_{t_1}^{t_2}(\Pi_s - \Pi_P)dt = 0 \tag{14}$$

and taking the variations of u, v, w, ψ_x and ψ_y integrating by parts, the non-classical governing differential equations can be derived as

$$\frac{\partial \bar{N}_{xx}}{\partial x} + \frac{\partial \bar{N}_{xy}}{\partial y} = 0 \tag{15a}$$

$$\frac{\partial \bar{N}_{xy}}{\partial x} + \frac{\partial \bar{N}_{yy}}{\partial y} = 0 \tag{15b}$$

$$\frac{\partial Q_x}{\partial x} + \frac{\partial Q_y}{\partial y} + \frac{\partial Q_x^s}{\partial x} + \frac{\partial Q_y^s}{\partial y} + \frac{\bar{N}_{yy}}{R} + \bar{N}_{xx}\frac{\partial^2(w+w^*)}{\partial x^2} + 2\bar{N}_{xy}\frac{\partial^2(w+w^*)}{\partial x \partial y} + \bar{N}_{yy}\frac{\partial^2(w+w^*)}{\partial y^2} + q = 0 \tag{15c}$$

$$\frac{\partial \bar{M}_{xx}}{\partial x} + \frac{\partial \bar{M}_{xy}}{\partial y} - Q_x = 0 \tag{15d}$$

$$\frac{\partial \bar{M}_{xy}}{\partial x} + \frac{\partial \bar{M}_{yy}}{\partial y} - Q_y = 0 \tag{15e}$$

The Airy stress function $f(x, y)$ can be introduced as

$$\bar{N}_{xx} = \frac{\partial^2 f}{\partial y^2}, \bar{N}_{yy} = \frac{\partial^2 f}{\partial x^2}, \bar{N}_{xy} = -\frac{\partial^2 f}{\partial x \partial y} \tag{16}$$

As a result, the strain components can be expressed as

$$\varepsilon_{xx}^{0} = -\varphi_2\frac{\partial^2 f}{\partial x^2} + \varphi_1\frac{\partial^2 f}{\partial y^2} + 2\tau_s\varphi_2\frac{w+w^*}{R} - \frac{2\tau_s}{A_{11}^{*}+A_{12}^{*}} + \tau_s\varphi_1\left(\frac{\partial(w+w^*)}{\partial x}\right)^2 - \tau_s\varphi_2\left(\frac{\partial(w+w^*)}{\partial y}\right)^2 \tag{17a}$$

$$\varepsilon_{yy}^{0} = -\varphi_2\frac{\partial^2 f}{\partial y^2} + \varphi_1\frac{\partial^2 f}{\partial x^2} - 2\tau_s\varphi_1\frac{w+w^*}{R} - \frac{2\tau_s}{A_{11}^{*}+A_{12}^{*}} + \tau_s\varphi_1\left(\frac{\partial(w+w^*)}{\partial y}\right)^2 - \tau_s\varphi_2\left(\frac{\partial(w+w^*)}{\partial x}\right)^2 \tag{17b}$$

$$\gamma_{xy}^{0} = -\varphi_3\frac{\partial^2 f}{\partial x \partial y} + \tau_s\varphi_3\frac{\partial(w+w^*)}{\partial x}\frac{\partial(w+w^*)}{\partial y} \tag{17c}$$

in which

$$\varphi_1 = \frac{A_{11}^{*}}{(A_{11}^{*})^2 - (A_{12}^{*})^2}, \quad \varphi_2 = \frac{A_{12}^{*}}{(A_{11}^{*})^2 - (A_{12}^{*})^2}, \quad \varphi_3 = \frac{1}{A_{55}^{*}} \tag{18}$$

Also, the geometrical compatibility equation for an imperfect cylindrical shell is written as

$$\frac{\partial^2 \varepsilon_{xx}^{0}}{\partial y^2} + \frac{\partial^2 \varepsilon_{yy}^{0}}{\partial x^2} - \frac{\partial^2 \gamma_{xy}^{0}}{\partial x \partial y} = \left(\frac{\partial^2 w}{\partial x \partial y}\right)^2 - \frac{\partial^2 w}{\partial x^2}\frac{\partial^2 w}{\partial y^2} + 2\frac{\partial^2 w}{\partial x \partial y}\frac{\partial^2 w^*}{\partial x \partial y} - \frac{\partial^2 w}{\partial x^2}\frac{\partial^2 w^*}{\partial y^2} - \frac{\partial^2 w}{\partial y^2}\frac{\partial^2 w^*}{\partial x^2} - \frac{1}{R}\frac{\partial^2 w}{\partial x^2} \tag{19}$$

From differential equations of (15c) and (19) and with the aid of equations (10) and (17), the nonlinear size-dependent governing differential equations in terms of f, w, ψ_x, and ψ_y can be expressed as

$$-D_{11}^{*}\frac{\partial^3 \psi_x}{\partial x^3} + \varphi_4\frac{\partial^3 \psi_x}{\partial x \partial y^2} - D_{11}^{*}\frac{\partial^3 \psi_y}{\partial y^3} + \varphi_4\frac{\partial^3 \psi_y}{\partial x^2 \partial y} - E_{11}^{*}\left(\frac{\partial^4 w}{\partial x^4} + 2\frac{\partial^4 w}{\partial x^2 \partial y^2} + \frac{\partial^4 w}{\partial y^4}\right) - 2\tau_s\left(\frac{\partial^2 w}{\partial x^2} + \frac{\partial^2 w}{\partial y^2}\right) - \frac{1}{R}\frac{\partial^2 f}{\partial x^2} = \frac{\partial^2(w+w^*)}{\partial x^2}\frac{\partial^2 f}{\partial y^2} - 2\frac{\partial^2(w+w^*)}{\partial x \partial y}\frac{\partial^2 f}{\partial x \partial y} + \frac{\partial^2(w+w^*)}{\partial y^2}\frac{\partial^2 f}{\partial x^2} + q \tag{20a}$$

$$\varphi_1\frac{\partial^4 f}{\partial x^4} + (\varphi_3 - 2\varphi_2)\frac{\partial^4 f}{\partial x^2 \partial y^2} + \varphi_1\frac{\partial^4 f}{\partial y^4} + \frac{2\tau_s}{R}\left(-\varphi_1\frac{\partial^2 w}{\partial x^2} + \varphi_2\frac{\partial^2 w}{\partial y^2}\right) + \frac{1}{R}\frac{\partial^2 w}{\partial x^2} = \left(\frac{\partial^2(w+w^*)}{\partial x \partial y}\right)^2 - \frac{\partial^2(w+w^*)}{\partial x^2}\frac{\partial^2(w+w^*)}{\partial y^2}$$

$$-2\tau_s\varphi_1\left(\frac{\partial^3(w+w^*)}{\partial x\partial y^2}\frac{\partial(w+w^*)}{\partial x}+2\left(\frac{\partial^2(w+w^*)}{\partial x\partial y}\right)^2+\frac{\partial^3(w+w^*)}{\partial x^2\partial y}\frac{\partial(w+w^*)}{\partial y}\right)+2\tau_s\varphi_2\left(\frac{\partial^3(w+w^*)}{\partial x^3}\frac{\partial(w+w^*)}{\partial x}+\frac{\partial^3(w+w^*)}{\partial y^3}\frac{\partial(w+w^*)}{\partial y}+\left(\frac{\partial^2(w+w^*)}{\partial x^2}\right)^2+\left(\frac{\partial^2(w+w^*)}{\partial y^2}\right)^2\right)+\tau_s\varphi_3\left(\frac{\partial^3(w+w^*)}{\partial x^2\partial y}\frac{\partial(w+w^*)}{\partial y}\frac{\partial^2(w+w^*)}{\partial x^2}\frac{\partial^2(w+w^*)}{\partial y^2}+\left(\frac{\partial^2(w+w^*)}{\partial x\partial y}\right)^2+\frac{\partial(w+w^*)}{\partial x}\frac{\partial^3(w+w^*)}{\partial x\partial y^2}\right) \tag{20b}$$

$$D_{11}^*\frac{\partial^2\psi_x}{\partial x^2}+D_{55}^*\frac{\partial^2\psi_x}{\partial y^2}-k_sA_{55}^*\left(\psi_x+\frac{\partial w}{\partial x}\right)+\varphi_5\frac{\partial^2\psi_y}{\partial x\partial y}+E_{11}^*\left(\frac{\partial^3 w}{\partial x^3}+\frac{\partial^3 w}{\partial x\partial y^2}\right)=0 \tag{20c}$$

$$D_{11}^*\frac{\partial^2\psi_y}{\partial y^2}+D_{55}^*\frac{\partial^2\psi_y}{\partial x^2}-k_sA_{55}^*\left(\psi_y+\frac{\partial w}{\partial y}\right)+\varphi_5\frac{\partial^2\psi_x}{\partial x\partial y}+E_{11}^*\left(\frac{\partial^3 w}{\partial x^2\partial y}+\frac{\partial^3 w}{\partial y^3}\right)=0 \tag{20d}$$

where

$$\varphi_4=-D_{12}^*-2D_{55}^*,\quad \varphi_5=D_{12}^*+D_{55}^* \tag{21}$$

It is assumed that the end supports of nanoshell are simply supported or clamped. Therefore, the boundary conditions at $x=0, L$ can be expressed as:

For simply supported edge supports: $w=0,\quad \bar{M}_{xx}=0$

For clamped edge supports: $w=0,\quad \frac{\partial w}{\partial x}=0$

Additionally, it is clear that

$$\int_0^{2\pi R}\bar{N}_{xx}dy+\pi R^2q=0 \tag{22}$$

Moreover, the closed condition (periodicity) can be given as follows

$$\int_0^{2\pi R}\frac{\partial v}{\partial y}dy=0 \tag{23a}$$

which yields

$$\int_0^{2\pi R}\left(-\varphi_2\frac{\partial^2 f}{\partial y^2}+\varphi_1\frac{\partial^2 f}{\partial x^2}-2\tau_s\varphi_1\frac{w+w^*}{R}-\frac{2\tau_s}{A_{11}^*+A_{12}^*}+\tau_s\varphi_1\left(\frac{\partial(w+w^*)}{\partial y}\right)^2-\tau_s\varphi_2\left(\frac{\partial(w+w^*)}{\partial x}\right)^2+\frac{w+w^*}{R}-\frac{1}{2}\left(\frac{\partial w}{\partial y}\right)^2-\frac{\partial w}{\partial y}\frac{\partial w^*}{\partial y}\right)dy=0 \tag{23b}$$

The average end shortening of nanoshell can be introduced as

$$\begin{aligned}\frac{\Delta_x}{L}&=-\frac{1}{2\pi RL}\int_0^{2\pi R}\int_0^L\frac{\partial u}{\partial x}dxdy\\&=-\frac{1}{2\pi RL}\int_0^{2\pi R}\int_0^L\left(-\varphi_2\frac{\partial^2 f}{\partial x^2}+\varphi_1\frac{\partial^2 f}{\partial y^2}+2\tau_s\varphi_2\frac{w+w^*}{R}-\frac{2\tau_s}{A_{11}^*+A_{12}^*}+\varphi_1\tau_s\left(\frac{\partial(w+w^*)}{\partial x}\right)^2-\varphi_2\tau_s\left(\frac{\partial(w+w^*)}{\partial y}\right)^2-\frac{1}{2}\left(\frac{\partial w}{\partial x}\right)^2-\frac{\partial w}{\partial x}\frac{\partial w^*}{\partial x}\right)dxdy\end{aligned} \tag{24}$$

3. Solution procedure

3.1. Boundary layer-type governing equations

In order to perform the solution methodology, the following dimensionless parameters are defined

$$\begin{aligned}&X=\frac{\pi x}{L},\quad Y=\frac{y}{R},\quad \beta=\frac{L}{\pi R},\quad \eta=\frac{L^2}{\pi^2h^2},\quad \epsilon=\frac{\pi^2Rh}{L^2}\\&\{a_{11}^*,a_{12}^*,a_{55}^*,d_{11}^*,d_{12}^*,d_{55}^*,e_{11}^*\}=\left\{\frac{A_{11}^*}{A_{110}},\frac{A_{12}^*}{A_{110}},\frac{A_{55}^*}{A_{110}},\frac{D_{11}^*}{A_{110}h^2},\frac{D_{12}^*}{A_{110}h^2},\frac{D_{55}^*}{A_{110}h^2},\frac{E_{11}^*}{A_{110}h^2}\right\}\\&\{W,W^*\}=\frac{\epsilon}{h}\{w,w^*\},\quad F=\frac{\epsilon^2 f}{A_{110}h^2},\quad \{\Psi_x,\ \Psi_y\}=\frac{\epsilon^2L}{\pi h}\{\psi_x,\ \psi_y\},\quad \bar{\tau}=\frac{\tau_s}{A_{110}}\\&\{\mathcal{M}_{xx},\mathcal{M}_{yy}\}=\frac{\epsilon^2L^2\{\bar{M}_{xx},\bar{M}_{yy}\}}{\pi^2A_{110}h^3},\quad \mathcal{P}_q=\frac{3^{3/4}qLR^{3/2}}{4\pi A_{110}h^{3/2}},\\&\delta_q=\frac{3^{3/4}\Delta_x\sqrt{R}}{4\pi h^{3/2}}\end{aligned} \tag{25}$$

in which $A_{110}=(\lambda+2\mu)h$. Now, by introducing the below derivative operators

$$\begin{aligned}\mathcal{L}_{11}(\,)&=-e_{11}^*\frac{\partial^4}{\partial X^4}-2e_{11}^*\beta^2\frac{\partial^4}{\partial X^2\partial Y^2}-e_{11}^*\beta^4\frac{\partial^4}{\partial Y^4}\\\mathcal{L}_{12}(\,)&=-\eta\frac{\partial^2}{\partial X^2}-\eta\beta^2\frac{\partial^2}{\partial Y^2}\\\mathcal{L}_{13}(\,)&=-d_{11}^*\frac{\partial^3}{\partial X^3}+\vartheta_4\beta^2\frac{\partial^3}{\partial X\partial Y^2}\\\mathcal{L}_{14}(\,)&=-d_{11}^*\beta^3\frac{\partial^3}{\partial Y^3}+\vartheta_4\beta\frac{\partial^3}{\partial X^2\partial Y}\\\mathcal{L}_{21}(\,)&=\vartheta_1\frac{\partial^4}{\partial X^4}+(\vartheta_3-2\vartheta_2)\beta^2\frac{\partial^4}{\partial X^2\partial Y^2}+\vartheta_1\beta^4\frac{\partial^4}{\partial Y^4}\\\mathcal{L}_{22}(\,)&=-\vartheta_1\frac{\partial^2}{\partial X^2}+\vartheta_2\beta^2\frac{\partial^2}{\partial Y^2}\\\mathcal{L}_{31}(\,)&=-k_sa_{55}^*\frac{\partial}{\partial X}+e_{11}^*\frac{\partial^3}{\partial X^3}+e_{11}^*\beta^2\frac{\partial^3}{\partial X\partial Y^2}\\\mathcal{L}_{32}(\,)&=-k_sa_{55}^*+d_{11}^*\frac{\partial^2}{\partial X^2}+d_{55}^*\beta^2\frac{\partial^2}{\partial Y^2}\\\mathcal{L}_{41}(\,)&=-k_sa_{55}^*\beta\frac{\partial}{\partial Y}+e_{11}^*\beta\frac{\partial^3}{\partial X^2\partial Y}+e_{11}^*\beta^3\frac{\partial^3}{\partial Y^3}\\\mathcal{L}_{42}(\,)&=-k_sa_{55}^*+d_{55}^*\frac{\partial^2}{\partial X^2}+d_{11}^*\beta^2\frac{\partial^2}{\partial Y^2}\\\tilde{\mathcal{L}}_1(\,)&=\frac{\partial^2}{\partial X^2}\frac{\partial^2}{\partial Y^2}-2\frac{\partial^2}{\partial X\partial Y}\frac{\partial^2}{\partial X\partial Y}+\frac{\partial^2}{\partial Y^2}\frac{\partial^2}{\partial X^2}\\\tilde{\mathcal{L}}_2(\,)&=\frac{\partial^3}{\partial X\partial Y^2}\frac{\partial}{\partial X}+\frac{\partial}{\partial X}\frac{\partial^3}{\partial X\partial Y^2}+4\frac{\partial^2}{\partial X\partial Y}\frac{\partial^2}{\partial X\partial Y}+\frac{\partial}{\partial Y}\frac{\partial^3}{\partial X^2\partial Y}+\frac{\partial^3}{\partial X^2\partial Y}\frac{\partial}{\partial Y}\\\tilde{\mathcal{L}}_3(\,)&=\frac{\partial^3}{\partial X^3}\frac{\partial}{\partial X}+\frac{\partial}{\partial X}\frac{\partial^3}{\partial X^3}+\beta^4\frac{\partial^3}{\partial Y^3}\frac{\partial}{\partial Y}+\beta^4\frac{\partial}{\partial Y}\frac{\partial^3}{\partial Y^3}+2\frac{\partial^2}{\partial X^2}\frac{\partial^2}{\partial X^2}+2\beta^4\frac{\partial^2}{\partial Y^2}\frac{\partial^2}{\partial Y^2}\\\tilde{\mathcal{L}}_4(\,)&=\frac{\partial^2}{\partial X^2}\frac{\partial^2}{\partial Y^2}+2\frac{\partial^2}{\partial X\partial Y}\frac{\partial^2}{\partial X\partial Y}+\frac{\partial^2}{\partial Y^2}\frac{\partial^2}{\partial X^2}+\frac{\partial^3}{\partial X^2\partial Y}\frac{\partial}{\partial Y}+\frac{\partial}{\partial Y}\frac{\partial^3}{\partial X^2\partial Y}+\frac{\partial}{\partial X}\frac{\partial^3}{\partial X\partial Y^2}+\frac{\partial^3}{\partial X\partial Y^2}\frac{\partial}{\partial X}\end{aligned} \tag{26}$$

the dimensionless form of the size-dependent nonlinear governing differential equations can be expressed as

$$\epsilon^2\mathcal{L}_{11}(W)+\epsilon^2 2\bar{\tau}\mathcal{L}_{12}(W)+\epsilon\mathcal{L}_{13}(\Psi_x)+\epsilon\mathcal{L}_{14}(\Psi_y)-\frac{\partial^2 F}{\partial X^2}=\beta^2\tilde{\mathcal{L}}_1(W+W^*,F)+\epsilon^{3/2}\frac{4}{3}3^{1/4}\mathcal{P}_q \tag{27a}$$

$$\mathcal{L}_{21}(F)+2\bar{\tau}\mathcal{L}_{22}(W)+\frac{\partial^2 W}{\partial X^2}=-\frac{\beta^2}{2}\tilde{\mathcal{L}}_1(W+2W^*,W)-\bar{\tau}\beta^2\tilde{\mathcal{L}}_2(W+2W^*,W)+\bar{\tau}\vartheta_1\tilde{\mathcal{L}}_3(W+2W^*,W)+\frac{\bar{\tau}\vartheta_2\beta^2}{2}\tilde{\mathcal{L}}_4(W+2W^*,W) \tag{27b}$$

$$\epsilon\mathcal{L}_{31}(W)+\mathcal{L}_{32}(\Psi_x)+\vartheta_5\beta\frac{\partial^2\Psi_y}{\partial X\partial Y}=0 \tag{27c}$$

$$\epsilon\mathcal{L}_{41}(W)+\mathcal{L}_{42}(\Psi_y)+\vartheta_5\beta\frac{\partial^2\Psi_x}{\partial X\partial Y}=0 \tag{27d}$$

where

$$\vartheta_1=\frac{a_{11}^*}{(a_{11}^*)^2-(a_{12}^*)^2},\quad \vartheta_2=\frac{a_{12}^*}{(a_{11}^*)^2-(a_{12}^*)^2},\quad \vartheta_3=\frac{1}{a_{55}^*}$$
$$\vartheta_4=-d_{12}^*-2d_{55}^*,\quad \vartheta_5=d_{12}^*+d_{55}^* \tag{28}$$

Additionally, the boundary conditions in dimensionless form will be at $X=0,\pi$

For simply supported edge supports: $W=0,\quad \mathcal{M}_{xx}=0$

For clamped edge supports: $W=0,\ \frac{\partial W}{\partial X}=0$

Also, one will have

$$\frac{1}{2\pi}\int_0^{2\pi}\beta^2\frac{\partial^2 F}{\partial Y^2}dY+\frac{2}{3}3^{1/4}\epsilon^{3/2}\mathcal{P}_q P=0 \tag{29}$$

and the closed condition becomes

$$\int_0^{2\pi}\left(-\vartheta_2\frac{\partial^2 F}{\partial Y^2}+\vartheta_1\frac{\partial^2 F}{\partial X^2}+(1-2\bar{\tau}\vartheta_1)(W+W^*)-\bar{\tau}\vartheta_2\left(\frac{\partial(W+W^*)}{\partial X}\right)^2+(1-2\bar{\tau}\vartheta_1)\left(\frac{\partial(W+W^*)}{\partial Y}\right)^2-2\bar{\tau}\vartheta_6(\vartheta_1-\vartheta_2)\epsilon\right)dY=0 \tag{30}$$

In addition, the unit end shortening of nanoshell is achieved as

$$\delta_q=-\frac{3^{3/4}}{8\pi^2\varepsilon^{3/2}}\int_0^{2\pi}\int_0^{\pi}\left(\vartheta_1\beta^2\frac{\partial^2 F}{\partial Y^2}-\vartheta_2\frac{\partial^2 F}{\partial X^2}+2\bar{\tau}\vartheta_2(W+W^*)-\frac{1}{2}(1-2\bar{\tau}\vartheta_1)\left(\frac{\partial(W+W^*)}{\partial X}\right)^2-\bar{\tau}\vartheta_2\beta^2\left(\frac{\partial(W+W^*)}{\partial Y}\right)^2-2\bar{\tau}\vartheta_6(\vartheta_1-\vartheta_2)\epsilon\right)dXdY \tag{31}$$

where $\vartheta_6=R/h$.

3.2. *Singular perturbation technique*

In the preceding subsection, the important parameter ε was introduced. It has been revealed that practically, for the shell structure, one will have $\frac{L^2}{Rh}\geq 20$, so $\varepsilon<1$ will always be true. Therefore, equation (27) represent the boundary layer type equations which consider both the nonlinear prebuckling deformations and large deflections in the postbuckling domain in conjunction with the effect of surface stress. Now, by assuming ε as a small perturbation parameter, the singular perturbation technique can be put into use, which has been successfully applied to the nonlinear analyses of cylindrical shells at macroscale [54-58]. On the basis of this technique, it is assumed that

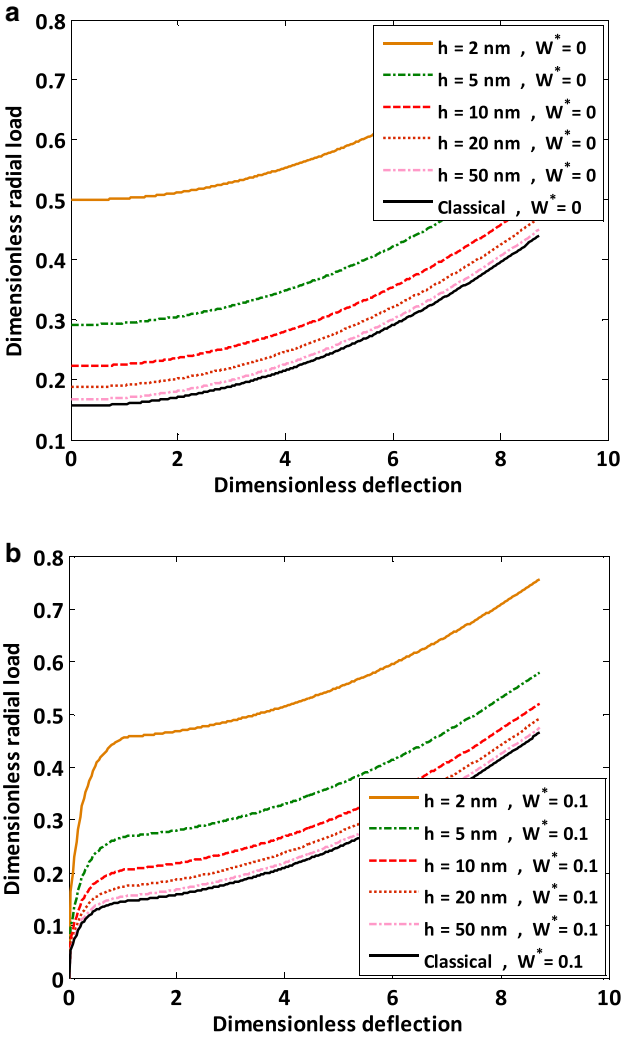

Fig. 2 – Dimensionless postbuckling load-deflection curves of nanoshells corresponding to various shell thicknesses: (a) perfect nanoshell, (b) imperfect nanoshell ($L^2/Rh = 200$, $R/h = 50$).

$$W=\bar{W}(X,Y,\epsilon)+\tilde{W}(X,Y,\epsilon,\xi)+\hat{W}(X,Y,\epsilon,\varsigma) \tag{32a}$$

$$F=\bar{F}(X,Y,\epsilon)+\tilde{F}(X,Y,\epsilon,\xi)+\hat{F}(X,Y,\epsilon,\varsigma) \tag{32b}$$

$$\Psi_x=\bar{\Psi}_x(X,Y,\epsilon)+\tilde{\Psi}_x(X,Y,\epsilon,\xi)+\hat{\Psi}_x(X,Y,\epsilon,\varsigma) \tag{32c}$$

$$\Psi_y=\bar{\Psi}_y(X,Y,\epsilon)+\tilde{\Psi}_y(X,Y,\epsilon,\xi)+\hat{\Psi}_y(X,Y,\epsilon,\varsigma) \tag{32d}$$

where $\bar{W}(X,Y,\epsilon)$, $\bar{F}(X,Y,\epsilon)$, $\bar{\Psi}_x(X,Y,\epsilon)$, $\bar{\Psi}_y(X,Y,\epsilon)$ denote regular solutions of the nanoshell, $\tilde{W}(X,Y,\epsilon,\xi)$, $\tilde{F}(X,Y,\epsilon,\xi)$, $\tilde{\Psi}_x(X,Y,\epsilon,\xi)$, $\tilde{\Psi}_y(X,Y,\epsilon,\xi)$ and $\hat{W}(X,Y,\epsilon,\varsigma)$, $\hat{F}(X,Y,\epsilon,\varsigma)$, $\hat{\Psi}_x(X,Y,\epsilon,\varsigma)$, are the boundary layer solutions corresponding to $X=0$

Table 1 – Material properties of a cylindrical nanoshell made of silicon [59,60].

E(GPa)	210
ν	0.24
μ_s(N/m)	−2.774
λ_s(N/m)	−4.488
τ_s(N/m)	0.6048

Table 2 – Comparison of the critical buckling pressures of isotropic cylindrical shells with clamped edge supports subjected to lateral pressure ($\nu = 0.3$, $E = 200$ GPa).

L/R	R/h	Present work (Pa)	Ref. [61] (Pa)
2	300	84991.09	85860
	3000	275.82	276.5
5	300	32897.22	32954
	3000	108.13	109

and $X = \pi$, respectively. These solutions can be expressed in the forms of perturbation expansions below

$$\bar{W}(X,Y,\epsilon) = \sum_{i=0} \epsilon^{i/2}\bar{W}_{i/2}(X,Y), \quad \bar{F}(X,Y,\epsilon) = \sum_{i=0} \epsilon^{i/2}\bar{F}_{i/2}(X,Y)$$

$$\bar{\Psi}_x(X,Y,\epsilon) = \sum_{i=1} \epsilon^{i/2}\bar{\Psi}_{x\,i/2}(X,Y), \quad \bar{\Psi}_y(X,Y,\epsilon) = \sum_{i=1} \epsilon^{i/2}\bar{\Psi}_{y\,i/2}(X,Y)$$

$$\tilde{W}(X,Y,\epsilon,\xi) = \sum_{i=0} \epsilon^{i/2+1}\tilde{W}_{i/2+1}(X,Y,\xi),$$

$$\tilde{F}(X,Y,\epsilon,\xi) = \sum_{i=0} \epsilon^{i/2+2}\tilde{F}_{i/2+2}(X,Y,\xi)$$

$$\tilde{\Psi}_x(X,Y,\epsilon,\xi) = \sum_{i=0} \epsilon^{(i+3)/2}\tilde{\Psi}_{x(i+3)/2}(X,Y,\xi),$$

$$\tilde{\Psi}_y(X,Y,\epsilon,\xi) = \sum_{i=0} \epsilon^{i/2+2}\tilde{\Psi}_{y\,i/2+2}(X,Y,\xi)$$

$$\hat{W}(X,Y,\epsilon,\varsigma) = \sum_{i=0} \epsilon^{i/2+1}\hat{W}_{i/2+1}(X,Y,\varsigma),$$

$$\hat{F}(X,Y,\epsilon,\varsigma) = \sum_{i=0} \epsilon^{i/2+2}\hat{F}_{i/2+2}(X,Y,\varsigma)$$

$$\hat{\Psi}_x(X,Y,\epsilon,\varsigma) = \sum_{i=0} \epsilon^{(i+3)/2}\hat{\Psi}_{x(i+3)/2}(X,Y,\varsigma),$$

$$\hat{\Psi}_y(X,Y,\epsilon,\varsigma) = \sum_{i=0} \epsilon^{i/2+2}\hat{\Psi}_{y\,i/2+2}(X,Y,\varsigma) \tag{33}$$

in which ξ and ς stand for boundary layer variables which are defined as

$$\xi = \frac{X}{\sqrt{\epsilon}}, \quad \varsigma = \frac{\pi - X}{\sqrt{\epsilon}} \tag{34}$$

Moreover, it is assumed that

$$\epsilon^{3/2}\frac{4}{3}3^{1/4}\,q = \sum_{i=0} \epsilon^{i}\mathcal{Q}_i \tag{35}$$

In order to determine the maximum order of ε which confirms the convergence of the solution procedure, an upper tolerance limit of 0.001 has been considered. It is observed that after the forth order (ε^4), the error is smaller than the tolerance limit.

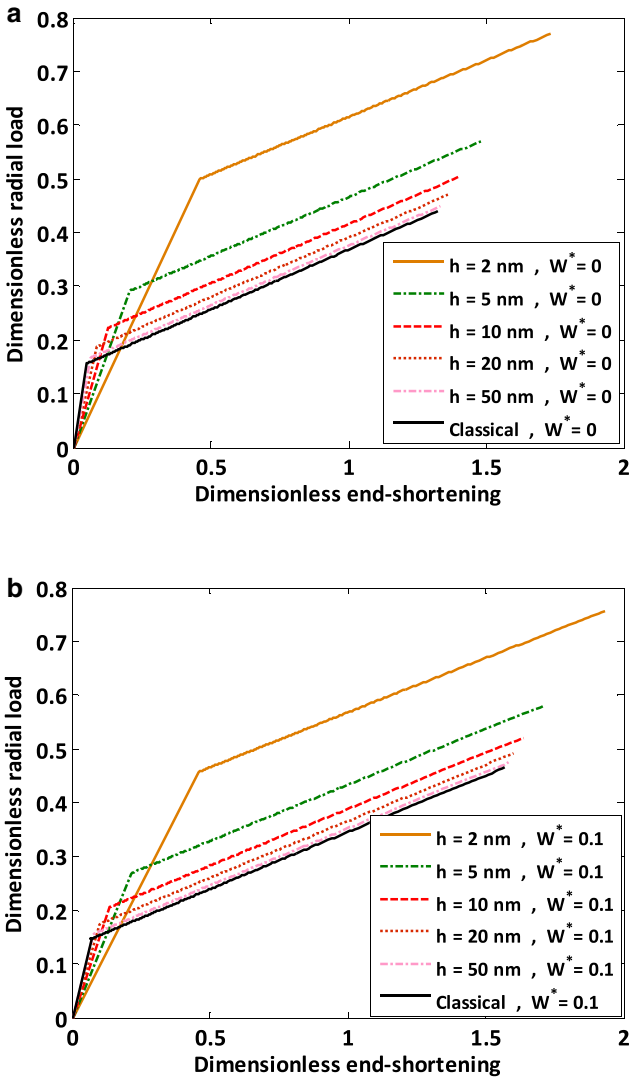

Fig. 3 – Dimensionless postbuckling load-shortening curves of nanoshells corresponding to various shell thicknesses: (a) perfect nanoshell, (b) imperfect nanoshell ($L^2/Rh = 200$, $R/h = 50$).

By inserting equations (32) and (33) into the size-dependent nonlinear governing differential equations (27) and collecting the expressions with the same order of ε, the sets of perturbation equations relevant to both the regular and boundary layer solutions will be derived, which are given in Appendix A. Afterwards, it is assumed that $\bar{W}_0(X,Y) = \mathcal{A}_{00}^{(0)}$, $\bar{W}_{1/2}(X,Y) = \bar{W}_1(X,Y) = 0$ and $\bar{W}_{3/2}(X,Y) = \mathcal{A}_{00}^{(3/2)}$, in addition to $\bar{F}_0(X,Y) = -\mathcal{B}_{00}^{(0)}(\beta^2X^2 + \frac{Y^2}{2})$, $\bar{F}_{1/2}(X,Y) = \bar{F}_{3/2}(X,Y) = 0$ and $\bar{F}_1(X,Y) = -\mathcal{B}_{00}^{(1)}(\beta^2X^2 + \frac{Y^2}{2})$. Moreover, the initial buckling mode and the initial geometric imperfection of the nanoshell are considered, respectively, as

$$\bar{W}_2(X,Y) = \mathcal{A}_{00}^{(2)} + \mathcal{A}_{11}^{(2)}\sin(mX)\sin(nY) \tag{36a}$$

$$W^*(X,Y,\epsilon) = \epsilon^2\mathcal{A}_{11}^{*}\sin(mX)\cos(nY) = \epsilon^2\ell\mathcal{A}_{11}^{(2)}\sin(mX)\cos(nY) \tag{36b}$$

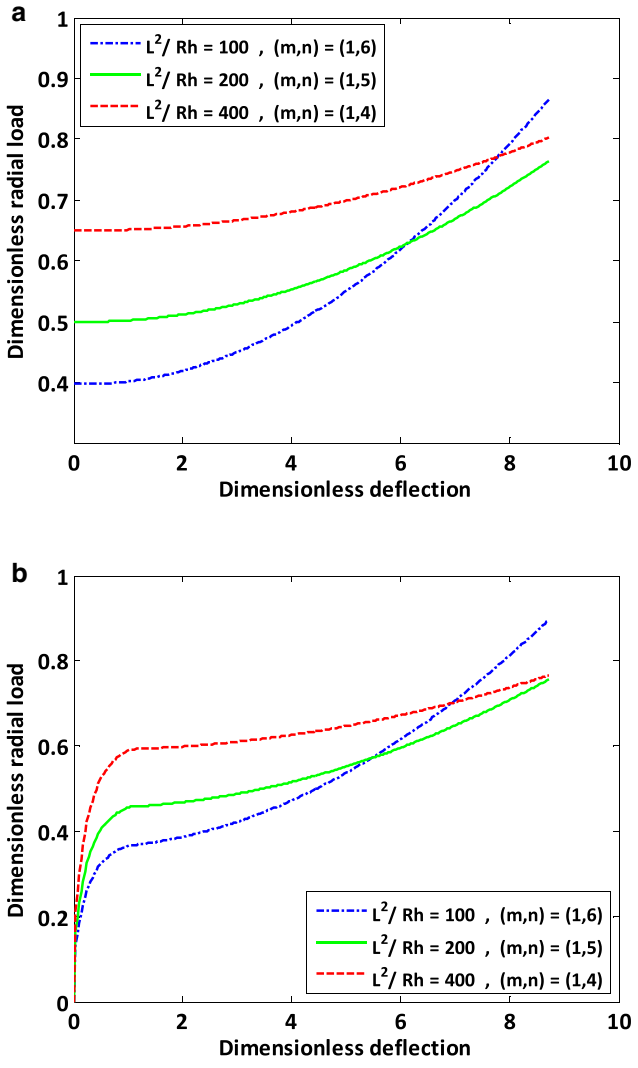

Fig. 4 – Dimensionless postbuckling load-deflection curves of nanoshells corresponding to various geometric parameters: (a) perfect nanoshell, (b) imperfect nanoshell (R/h = 50, h = 2 nm).

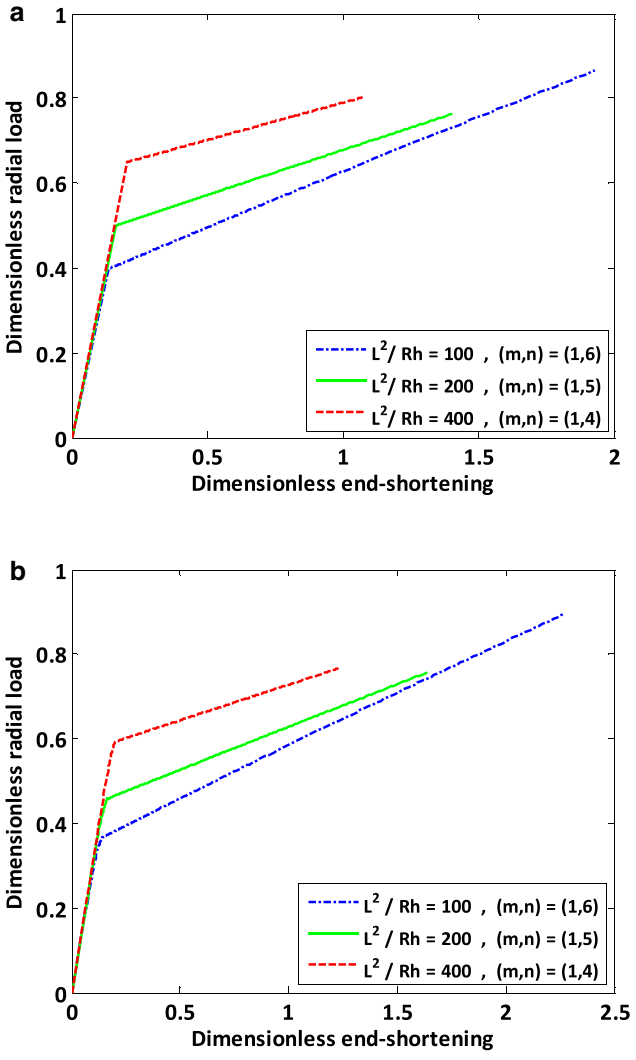

Fig. 5 – Dimensionless postbuckling load-shortening curves of nanoshells corresponding to various geometric parameters: (a) perfect nanoshell, (b) imperfect nanoshell (R/h = 50, h = 2 nm).

in which $\ell = \mathcal{A}_{11}^{*}/\mathcal{A}_{11}^{(2)}$ represents the imperfection parameter.

Now, by employing the given boundary, equation (29), closed conditions (30), and based on the unit end shortening (31), the postbuckling equilibrium paths can be derived as

$$\mathcal{P}_q = \frac{1}{2}3^{3/4}\epsilon^{-3/2}\left\{\mathcal{P}_q^{(0)} + \mathcal{P}_q^{(2)}\left(\mathcal{A}_{11}^{(2)}\epsilon^2\right)^2 + \ldots\right\} \tag{37}$$

and

$$\delta_q = \delta_q^{(0)} + \delta_q^{(2)}\left(\mathcal{A}_{11}^{(2)}\epsilon^2\right)^2 + \ldots \tag{38}$$

In accordance with the maximum dimensionless deflection of the nanoshell, $\mathcal{A}_{11}^{(2)}\epsilon^2$ is considered as the second perturbation parameter, which may be large in comparison with the first small perturbation parameter ε. If it is assumed that the maximum deflection occurs at the dimensionless point of $(X, Y) = (\pi/2m, \pi/2n)$, one will have

$$\mathcal{A}_{11}^{(2)}\epsilon^2 = \mathcal{W}_m + \mathcal{S}_1\mathcal{W}_m^2 + \ldots \tag{39}$$

in which $\mathcal{W}_m$ denotes the maximum dimensionless deflection of the nanoshell as

$$\mathcal{W}_m = \epsilon\frac{w_m}{h} + \mathcal{S}_2 \tag{40}$$

where the symbols $\mathcal{S}_1$ and $\mathcal{S}_2$ are given in Appendix A.

In order to determine the correct values of m and n corresponding to the maximum deflection, the minimum value of buckling load obtained by equation (37) should be calculated by taking $W = 0$ (noting that $\mathcal{W}_m \neq 0$).

4. Numerical results and discussion

Here, the size-dependent postbuckling equilibrium paths of perfect and imperfect cylindrical shear deformable nanoshells subjected to axial compression are presented considering the surface stress effects. The results presented in this section contain two parts. In the first part including Figures 2–5,

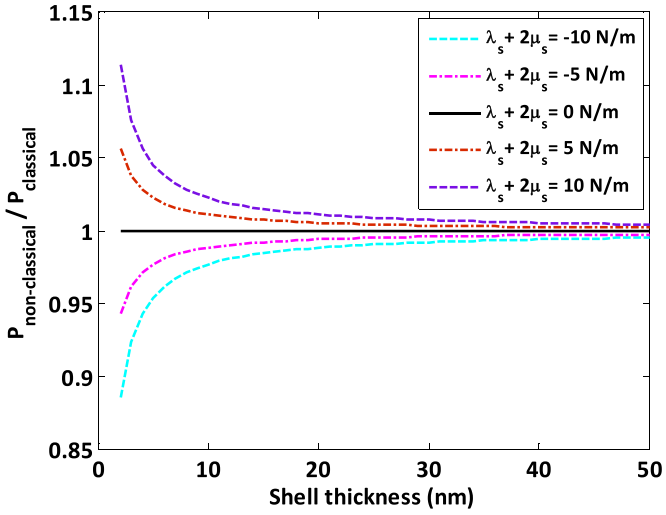

Fig. 6 – Variation of the critical buckling load ratio with nanoshell thickness corresponding to various surface elastic constants ($L^2/Rh = 200$, $R/h = 50$, $\tau_s = 0$ N/m).

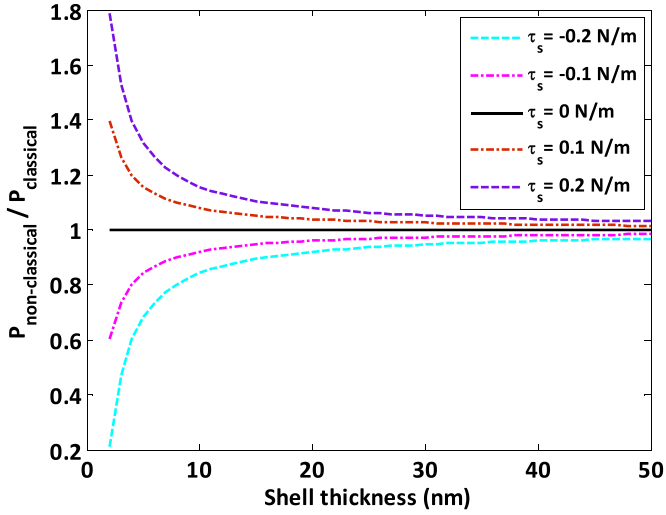

Fig. 7 – Variation of the critical buckling load ratio with nanoshell thickness corresponding to various residual surface stresses ($L^2/Rh = 200$, $R/h = 50$, $\lambda_s = \mu_s = 0$ N/m).

the results are obtained for a nanoshell made of silicon, the material properties of which are tabulated in Table 1. But in the second part of the numerical results including Figures 6 and 7, in order to demonstrate the influence of the value of surface elastic parameters on the critical buckling load of nanoshells, it is assumed that the naoshells are made of different materials with various surface elastic parameters. Also, in all the preceding numerical results, it is assumed that the edge supports of nanoshells are clamped.

At first, the validity as well as the accuracy of the present solution methodology is checked. Because in accordance with the authors' knowledge, there is no investigation available in published literature in which the buckling or postbuckling behavior of nanoshells is studied in the presence of surface stress effects, by ignoring the nonlinear and surface elasticity terms, the critical buckling load of a cylindrical shell at usual scale subjected to lateral pressure is calculated based on the present solution procedure and is compared with that of Mirfakhraei and Redekop [61] using differential quadrature numerical method. In Table 2, the critical buckling pressures of cylindrical shells with clamped edge supports obtained by the two different methods are compared corresponding to the same material and geometric properties. A very good agreement is found, which confirms the validity of the current analysis.

Plotted in Figure 2 are the classical and non-classical dimensionless postbuckling load-deflection equilibrium curves of perfect and imperfect cylindrical shear deformable

nanoshells made of silicon under hydrostatic pressure. It is revealed that through decreasing the value of shell thickness, the gap between classical and non-classical curves increases. It means that the surface free energy effects on the postbuckling characteristics of nanoshells with lower thickness are more prominent. This anticipation is the same for both the perfect and imperfect nanoshells.

The classical and non-classical dimensionless postbuckling load-shortening equilibrium curves of Silicon shear deformable nanoshells with and without initial geometric imperfection are depicted in Figure 3. It can be seen again that by decreasing the value of shell thickness, the effects of surface free energy on the postbuckling behavior of cylindrical nanoshells increase. Furthermore, it is found that the surface free energy effects cause increases in both the critical buckling pressure and critical end-shortening of nanoshell made of silicon. In addition, through a comparison of load-shortening curves related to the perfect and imperfect nanoshells, it can be observed that the initial geometric imperfection leads to decreases in both the critical buckling load and critical end-shortening of nanoshell subjected to radial compression.

Figure 4 illustrates the size-dependent dimensionless postbuckling load-deflection curves of cylindrical shear deformable nanoshells with various geometric parameters subjected to hydrostatic pressure. It is demonstrated that by increasing the value of L^2/Rh, the size-dependent dimensionless critical buckling pressure of nanoshell increases. Also, the slope of the variation of applied radial compressive load with deflection of nanoshell is lower in the postbuckling regime. Additionally, in the case of imperfect nanoshells, it is seen that the deflection of nanoshell corresponding to the prebuckling domain increases with higher values of L^2/Rh.

Presented in Figure 5 are the size-dependent dimensionless postbuckling load-shortening curves of cylindrical shear deformable nanoshells with and without initial geometric imperfection under radial compressive load relevant to various geometric parameters. It is observed that for both the perfect and imperfect nanoshells, increasing the value of L^2/Rh leads to higher dimensionless critical buckling pressure and higher dimensionless critical end-shortening. Also, it can be seen that by increasing the value of L^2/Rh, the slope of the postbuckling part of dimensionless load-shortening equilibrium path of nanoshell decreases.

Figures 6 and 7 show the variation of the ratio of non-classical buckling load to classical buckling load with the value of nanoshell thickness corresponding to different values of surface elastic constants and residual surface stress, respectively. It can be found that the effects of surface free energy including surface elasticity and residual surface stress may either increase or decrease the stiffness of cylindrical shear deformable nanoshell against compressive radial load, depending on the signs of surface properties. It is indicated that a positive value of surface elastic constant or residual surface stress causes to increase the size-dependent critical buckling pressure, whereas a negative one results in lower non-classical critical buckling load than that of the classical one. However, by increasing the value of nanoshell thickness, it can be seen that these effects diminish.

5. Conclusion

The objective of the present study was to predict the effects of surface free energy as one of the most important size effects on the nonlinear buckling and postbuckling behavior of cylindrical shear deformable nanoshells with and without initial geometric imperfections subjected to hydrostatic pressure. To this end, Gurtin-Murdoch elasticity theory was implemented into the first-order shear deformation shell theory to develop an efficient size-dependent shell model. Based upon the variational approach and using virtual work's principle, the non-classical governing differential equations were derived. Subsequently, a boundary layer theory was employed which considered simultaneously the effects of surface free energy, nonlinear prebuckling deformations, large postbuckling deflections and initial geometric imperfection. Finally, an efficient solution methodology based on a two-stepped singular perturbation technique was utilized to obtain the size-dependent critical buckling pressures and postbuckling equilibrium paths.

It was seen that through decreasing the value of nanoshell thickness, the gap between classical and non-classical curves increases, meaning that the surface free energy effects on the postbuckling characteristics of nanoshells with lower thickness were more prominent. Moreover, it was observed that surface free energy effects caused increases in both the critical buckling load and critical end-shortening of nanoshell made of silicon. Additionally, it was found that by increasing the value of L^2/Rh, the slope of variation of the applied radial compressive load with deflection of nanoshell was lower in the postbuckling regime, indicating that for both perfect and imperfect nanoshells, increasing the value of L^2/Rh led to higher dimensionless critical buckling pressure, and higher dimensionless critical end-shortening, and additionally led to a decrease in the slope of the postbuckling part of the dimensionless load-shortening equilibrium path of nanoshell. Furthermore, it was revealed that the effects of surface free energy including surface elasticity and residual surface stress could either increase or decrease the stiffness of cylindrical shear deformable nanoshell, depending on the signs of surface properties.

Appendix A

The sets of perturbation equations for the regular solutions are

$$O(\epsilon^0):\begin{cases} -\frac{\partial^2 \bar{F}_0}{\partial X^2} = \beta^2 \tilde{\mathcal{L}}_1(\bar{W}_0, \bar{F}_0) + \mathcal{Q}_0 \\ \mathcal{L}_{21}(\bar{F}_0) + 2\bar{\tau}\mathcal{L}_{22}(\bar{W}_0) + \frac{\partial^2 \bar{W}_0}{\partial X^2} = -\frac{\beta^2}{2}\tilde{\mathcal{L}}_1(\bar{W}_0, \bar{W}_0) \\ \quad -\bar{\tau}\beta^2\tilde{\mathcal{L}}_2(\bar{W}_0, \bar{W}_0) + \bar{\tau}\vartheta_1\tilde{\mathcal{L}}_3(\bar{W}_0, \bar{W}_0) + \frac{\bar{\tau}\vartheta_2\beta^2}{2}\tilde{\mathcal{L}}_4(\bar{W}_0, \bar{W}_0) \\ 0 = 0 \\ 0 = 0 \end{cases}$$

$$O(\epsilon^{1/2}):\begin{cases}-\frac{\partial^2\bar{F}_{1/2}}{\partial X^2}=\beta^2\tilde{\mathcal{L}}_1(\bar{W}_{1/2},\bar{F}_0)+\beta^2\tilde{\mathcal{L}}_1(\bar{W}_0,\bar{F}_{1/2})\\ \mathcal{L}_{21}(\bar{F}_{1/2})+2\bar{\tau}\mathcal{L}_{22}(\bar{W}_{1/2})+\frac{\partial^2\bar{W}_{1/2}}{\partial X^2}\\ \quad=-\frac{\beta^2}{2}\tilde{\mathcal{L}}_1(\bar{W}_0,\bar{W}_{1/2})-\bar{\tau}\vartheta_1\beta^2\tilde{\mathcal{L}}_2(\bar{W}_0,\bar{W}_{1/2})\\ \quad+\bar{\tau}\vartheta_2\tilde{\mathcal{L}}_3(\bar{W}_0,\bar{W}_{1/2})+\frac{\bar{\tau}\vartheta_3\beta^2}{2}\tilde{\mathcal{L}}_4(\bar{W}_0,\bar{W}_{1/2})\\ \mathcal{L}_{32}(\bar{\Psi}_{x_{1/2}})+\vartheta_5\beta\frac{\partial^2\bar{\Psi}_{y_{1/2}}}{\partial X\partial Y}=0\\ \mathcal{L}_{42}(\bar{\Psi}_{y_{1/2}})+\vartheta_5\beta\frac{\partial^2\bar{\Psi}_{x_{1/2}}}{\partial X\partial Y}=0\end{cases}$$

$$O(\epsilon^{1}):\begin{cases}-\frac{\partial^2\bar{F}_1}{\partial X^2}=\beta^2\tilde{\mathcal{L}}_1(\bar{W}_{1/2},\bar{F}_{1/2})+\beta^2\tilde{\mathcal{L}}_1(\bar{W}_1,\bar{F}_0)\\ \quad+\beta^2\tilde{\mathcal{L}}_1(\bar{W}_0,\bar{F}_1)+\mathcal{Q}_1\\ \mathcal{L}_{21}(\bar{F}_2)+2\bar{\tau}\mathcal{L}_{22}(\bar{W}_2)+\frac{\partial^2\bar{W}_2}{\partial X^2}=-\frac{\beta^2}{2}\tilde{\mathcal{L}}_1(\bar{W}_0,\bar{W}_2)\\ \quad-\frac{\beta^2}{2}\tilde{\mathcal{L}}_1(\bar{W}_{1/2},\bar{W}_{3/2})-\frac{\beta^2}{2}\tilde{\mathcal{L}}_1(\bar{W}_1,\bar{W}_1)\\ \quad-\bar{\tau}\vartheta_1\beta^2\tilde{\mathcal{L}}_2(\bar{W}_{1/2},\bar{W}_{1/2})+\bar{\tau}\vartheta_2\tilde{\mathcal{L}}_3(\bar{W}_0,\bar{W}_1)\\ \quad+\bar{\tau}\vartheta_2\tilde{\mathcal{L}}_3(\bar{W}_{1/2},\bar{W}_{1/2})+\frac{\bar{\tau}\vartheta_3\beta^2}{2}\tilde{\mathcal{L}}_4(\bar{W}_0,\bar{W}_1)\\ \quad+\frac{\bar{\tau}\vartheta_3\beta^2}{2}\tilde{\mathcal{L}}_4(\bar{W}_{1/2},\bar{W}_{1/2})\\ \mathcal{L}_{31}(\bar{W}_0)+\mathcal{L}_{32}(\bar{\Psi}_{x_1})+\vartheta_5\beta\frac{\partial^2\bar{\Psi}_{y_1}}{\partial X\partial Y}=0\\ \mathcal{L}_{41}(\bar{W}_0)+\mathcal{L}_{42}(\bar{\Psi}_{y_1})+\vartheta_5\beta\frac{\partial^2\bar{\Psi}_{x_1}}{\partial X\partial Y}=0\end{cases}$$

$$O(\epsilon^{3/2}):\begin{cases}-\frac{\partial^2\bar{F}_{3/2}}{\partial X^2}+\mathcal{L}_{13}(\bar{\Psi}_{x_{1/2}})+\mathcal{L}_{14}(\bar{\Psi}_{y_{1/2}})=\beta^2\tilde{\mathcal{L}}_1(\bar{W}_0,\bar{F}_{3/2})\\ \quad+\beta^2\tilde{\mathcal{L}}_1(\bar{W}_{1/2},\bar{F}_1)+\beta^2\tilde{\mathcal{L}}_1(\bar{W}_1,\bar{F}_{1/2})+\beta^2\tilde{\mathcal{L}}_1(\bar{W}_{3/2},\bar{F}_0)\\ \mathcal{L}_{21}(\bar{F}_{3/2})+2\bar{\tau}\mathcal{L}_{22}(\bar{W}_{3/2})+\frac{\partial^2\bar{W}_{3/2}}{\partial X^2}=-\frac{\beta^2}{2}\tilde{\mathcal{L}}_1(\bar{W}_0,\bar{W}_{3/2})\\ \quad-\frac{\beta^2}{2}\tilde{\mathcal{L}}_1(\bar{W}_{1/2},\bar{W}_1)-\bar{\tau}\vartheta_1\beta^2\tilde{\mathcal{L}}_2(\bar{W}_0,\bar{W}_{3/2})\\ \quad-\bar{\tau}\vartheta_1\beta^2\tilde{\mathcal{L}}_2(\bar{W}_{1/2},\bar{W}_1)+\bar{\tau}\vartheta_2\tilde{\mathcal{L}}_3(\bar{W}_0,\bar{W}_{3/2})\\ \quad+\bar{\tau}\vartheta_2\tilde{\mathcal{L}}_3(\bar{W}_{1/2},\bar{W}_1)\\ +\frac{\bar{\tau}\vartheta_3\beta^2}{2}\tilde{\mathcal{L}}_4(\bar{W}_0,\bar{W}_{3/2})+\frac{\bar{\tau}\vartheta_3\beta^2}{2}\tilde{\mathcal{L}}_4(\bar{W}_{1/2},\bar{W}_1)\\ \mathcal{L}_{31}(\bar{W}_{1/2})+\mathcal{L}_{32}(\bar{\Psi}_{x_{3/2}})+\vartheta_5\beta\frac{\partial^2\bar{\Psi}_{y_{3/2}}}{\partial X\partial Y}=0\\ \mathcal{L}_{41}(\bar{W}_{1/2})+\mathcal{L}_{42}(\bar{\Psi}_{y_{3/2}})+\vartheta_5\beta\frac{\partial^2\bar{\Psi}_{x_{3/2}}}{\partial X\partial Y}=0\end{cases}$$

$$O(\epsilon^{2}):\begin{cases}\mathcal{L}_{11}(\bar{W}_0)+2\bar{\tau}\mathcal{L}_{12}(\bar{W}_0)+\mathcal{L}_{13}(\bar{\Psi}_{x_1})+\mathcal{L}_{14}(\bar{\Psi}_{y_1})-\frac{\partial^2\bar{F}_2}{\partial X^2}\\ \quad=\beta^2\tilde{\mathcal{L}}_1(\bar{W}_0,\bar{F}_2)+\beta^2\tilde{\mathcal{L}}_1(\bar{W}_{1/2},\bar{F}_{3/2})\\ \quad+\beta^2\tilde{\mathcal{L}}_1(\bar{W}_1,\bar{F}_1)+\beta^2\tilde{\mathcal{L}}_1(\bar{W}_{3/2},\bar{F}_{1/2})\\ \quad+\beta^2\tilde{\mathcal{L}}_1(\bar{W}_2+W^*,\bar{F}_0)+\mathcal{Q}_2\\ \mathcal{L}_{21}(\bar{F}_2)+2\bar{\tau}\mathcal{L}_{22}(\bar{W}_2)+\frac{\partial^2\bar{W}_2}{\partial X^2}=-\frac{\beta^2}{2}\tilde{\mathcal{L}}_1(\bar{W}_0,\bar{W}_2+2W^*)\\ \quad-\frac{\beta^2}{2}\tilde{\mathcal{L}}_1(\bar{W}_{1/2},\bar{W}_{3/2})-\frac{\beta^2}{2}\tilde{\mathcal{L}}_1(\bar{W}_1,\bar{W}_1)\\ \quad-\bar{\tau}\vartheta_1\beta^2\tilde{\mathcal{L}}_2(\bar{W}_0,\bar{W}_2+2W^*)-\bar{\tau}\vartheta_1\beta^2\tilde{\mathcal{L}}_2(\bar{W}_{1/2},\bar{W}_{3/2})\\ \quad-\bar{\tau}\vartheta_1\beta^2\tilde{\mathcal{L}}_2(\bar{W}_1,\bar{W}_1)+\bar{\tau}\vartheta_2\tilde{\mathcal{L}}_3(\bar{W}_0,\bar{W}_2+2W^*)\\ \quad+\bar{\tau}\vartheta_2\tilde{\mathcal{L}}_3(\bar{W}_{1/2},\bar{W}_{3/2})+\bar{\tau}\vartheta_2\tilde{\mathcal{L}}_3(\bar{W}_1,\bar{W}_1)\\ \quad+\frac{\bar{\tau}\vartheta_3\beta^2}{2}\tilde{\mathcal{L}}_4(\bar{W}_0,\bar{W}_2+2W^*)+\frac{\bar{\tau}\vartheta_3\beta^2}{2}\tilde{\mathcal{L}}_4(\bar{W}_{1/2},\bar{W}_{3/2})\\ \quad+\frac{\bar{\tau}\vartheta_3\beta^2}{2}\tilde{\mathcal{L}}_4(\bar{W}_1,\bar{W}_1)\\ \mathcal{L}_{31}(\bar{W}_1)+\mathcal{L}_{32}(\bar{\Psi}_{x_2})+\vartheta_5\beta\frac{\partial^2\bar{\Psi}_{y_2}}{\partial X\partial Y}=0\\ \mathcal{L}_{41}(\bar{W}_1)+\mathcal{L}_{42}(\bar{\Psi}_{y_2})+\vartheta_5\beta\frac{\partial^2\bar{\Psi}_{x_2}}{\partial X\partial Y}=0\end{cases}$$

$$O(\epsilon^{5/2}):\begin{cases}\mathcal{L}_{11}(\bar{W}_{1/2})+2\bar{\tau}\mathcal{L}_{12}(\bar{W}_{1/2})+\mathcal{L}_{13}(\bar{\Psi}_{x_{3/2}})\\ \quad+\mathcal{L}_{14}(\bar{\Psi}_{y_{3/2}})-\frac{\partial^2\bar{F}_{5/2}}{\partial X^2}=\beta^2\tilde{\mathcal{L}}_1(\bar{W}_0,\bar{F}_{5/2})\\ \quad+\beta^2\tilde{\mathcal{L}}_1(\bar{W}_{1/2},\bar{F}_2)+\beta^2\tilde{\mathcal{L}}_1(\bar{W}_1,\bar{F}_{3/2})+\beta^2\tilde{\mathcal{L}}_1(\bar{W}_{3/2},\bar{F}_1)\\ \quad+\beta^2\tilde{\mathcal{L}}_1(\bar{W}_2+W^*,\bar{F}_{1/2})+\beta^2\tilde{\mathcal{L}}_1(\bar{W}_{5/2},\bar{F}_0)\\ \mathcal{L}_{21}(\bar{F}_{5/2})+2\bar{\tau}\mathcal{L}_{22}(\bar{W}_{5/2})+\frac{\partial^2\bar{W}_{5/2}}{\partial X^2}=-\frac{\beta^2}{2}\tilde{\mathcal{L}}_1(\bar{W}_0,\bar{W}_{5/2})\\ \quad-\frac{\beta^2}{2}\tilde{\mathcal{L}}_1(\bar{W}_{1/2},\bar{W}_2+2W^*)\\ -\frac{\beta^2}{2}\tilde{\mathcal{L}}_1(\bar{W}_1,\bar{W}_{3/2})-\bar{\tau}\vartheta_1\beta^2\tilde{\mathcal{L}}_2(\bar{W}_0,\bar{W}_{5/2})\\ \quad-\bar{\tau}\vartheta_1\beta^2\tilde{\mathcal{L}}_2(\bar{W}_{1/2},\bar{W}_2+2W^*)-\bar{\tau}\vartheta_1\beta^2\tilde{\mathcal{L}}_2(\bar{W}_1,\bar{W}_{3/2})\\ \quad+\bar{\tau}\vartheta_2\tilde{\mathcal{L}}_3(\bar{W}_0,\bar{W}_{5/2})+\bar{\tau}\vartheta_2\tilde{\mathcal{L}}_3(\bar{W}_{1/2},\bar{W}_2+2W^*)\\ +\bar{\tau}\vartheta_2\tilde{\mathcal{L}}_3(\bar{W}_1,\bar{W}_{3/2})+\frac{\bar{\tau}\vartheta_3\beta^2}{2}\tilde{\mathcal{L}}_4(\bar{W}_0,\bar{W}_{5/2})\\ \quad+\frac{\bar{\tau}\vartheta_3\beta^2}{2}\tilde{\mathcal{L}}_4(\bar{W}_{1/2},\bar{W}_2+2W^*)\\ +\frac{\bar{\tau}\vartheta_3\beta^2}{2}\tilde{\mathcal{L}}_4(\bar{W}_1,\bar{W}_{3/2})\\ \mathcal{L}_{31}(\bar{W}_{3/2})+\mathcal{L}_{32}(\bar{\Psi}_{x_{5/2}})+\vartheta_5\beta\frac{\partial^2\bar{\Psi}_{y_{5/2}}}{\partial X\partial Y}=0\\ \mathcal{L}_{41}(\bar{W}_{3/2})+\mathcal{L}_{42}(\bar{\Psi}_{y_{5/2}})+\vartheta_5\beta\frac{\partial^2\bar{\Psi}_{x_{5/2}}}{\partial X\partial Y}=0\end{cases}$$

$$O(\epsilon^{3}):\begin{cases}\mathcal{L}_{11}(\bar{W}_1)+2\bar{\tau}\mathcal{L}_{12}(\bar{W}_1)+\mathcal{L}_{13}(\bar{\Psi}_{x_2})+\mathcal{L}_{14}(\bar{\Psi}_{y_2})-\frac{\partial^2\bar{F}_3}{\partial X^2}\\ \quad=\beta^2\tilde{\mathcal{L}}_1(\bar{W}_0,\bar{F}_3)+\beta^2\tilde{\mathcal{L}}_1(\bar{W}_{1/2},\bar{F}_{5/2})\\ +\beta^2\tilde{\mathcal{L}}_1(\bar{W}_1,\bar{F}_2)+\beta^2\tilde{\mathcal{L}}_1(\bar{W}_{3/2},\bar{F}_{3/2})+\beta^2\tilde{\mathcal{L}}_1(\bar{W}_2+W^*,\bar{F}_1)\\ \quad+\beta^2\tilde{\mathcal{L}}_1(\bar{W}_{5/2},\bar{F}_{1/2})\\ +\beta^2\tilde{\mathcal{L}}_1(\bar{W}_3,\bar{F}_0)+\mathcal{Q}_3\\ \mathcal{L}_{21}(\bar{F}_3)+2\bar{\tau}\mathcal{L}_{22}(\bar{W}_3)+\frac{\partial^2\bar{W}_3}{\partial X^2}=-\frac{\beta^2}{2}\tilde{\mathcal{L}}_1(\bar{W}_0,\bar{W}_3)\\ \quad-\frac{\beta^2}{2}\tilde{\mathcal{L}}_1(\bar{W}_{1/2},\bar{W}_{5/2})-\frac{\beta^2}{2}\tilde{\mathcal{L}}_1(\bar{W}_1,\bar{W}_2+2W^*)\\ -\frac{\beta^2}{2}\tilde{\mathcal{L}}_1(\bar{W}_{3/2},\bar{W}_{3/2})-\bar{\tau}\vartheta_1\beta^2\tilde{\mathcal{L}}_2(\bar{W}_0,\bar{W}_3)\\ \quad-\bar{\tau}\vartheta_1\beta^2\tilde{\mathcal{L}}_2(\bar{W}_{1/2},\bar{W}_{5/2})\\ -\bar{\tau}\vartheta_1\beta^2\tilde{\mathcal{L}}_2(\bar{W}_1,\bar{W}_2+2W^*)-\bar{\tau}\vartheta_1\beta^2\tilde{\mathcal{L}}_2(\bar{W}_{3/2},\bar{W}_{3/2})\\ \quad+\bar{\tau}\vartheta_2\tilde{\mathcal{L}}_3(\bar{W}_0,\bar{W}_3)\\ +\bar{\tau}\vartheta_2\tilde{\mathcal{L}}_3(\bar{W}_{1/2},\bar{W}_{5/2})+\bar{\tau}\vartheta_2\tilde{\mathcal{L}}_3(\bar{W}_1,\bar{W}_2+2W^*)\\ \quad+\bar{\tau}\vartheta_2\tilde{\mathcal{L}}_3(\bar{W}_{3/2},\bar{W}_{3/2})+\frac{\bar{\tau}\vartheta_3\beta^2}{2}\tilde{\mathcal{L}}_4(\bar{W}_0,\bar{W}_3)\\ +\frac{\bar{\tau}\vartheta_3\beta^2}{2}\tilde{\mathcal{L}}_4(\bar{W}_{1/2},\bar{W}_{5/2})+\frac{\bar{\tau}\vartheta_3\beta^2}{2}\tilde{\mathcal{L}}_4(\bar{W}_1,\bar{W}_2+2W^*)\\ \quad+\frac{\bar{\tau}\vartheta_3\beta^2}{2}\tilde{\mathcal{L}}_4(\bar{W}_{3/2},\bar{W}_{3/2})\\ \mathcal{L}_{31}(\bar{W}_2)+\mathcal{L}_{32}(\bar{\Psi}_{x_3})+\vartheta_5\beta\frac{\partial^2\bar{\Psi}_{y_3}}{\partial X\partial Y}=0\\ \mathcal{L}_{41}(\bar{W}_2)+\mathcal{L}_{42}(\bar{\Psi}_{y_3})+\vartheta_5\beta\frac{\partial^2\bar{\Psi}_{x_3}}{\partial X\partial Y}=0\end{cases}$$

$$O(\epsilon^{7/2}):\begin{cases}\mathcal{L}_{11}(\bar{W}_{3/2})+2\bar{\tau}\mathcal{L}_{12}(\bar{W}_{3/2})+\mathcal{L}_{13}(\bar{\Psi}_{x_{5/2}})+\mathcal{L}_{14}(\bar{\Psi}_{y_{5/2}})\\ \quad-\frac{\partial^2\bar{F}_{7/2}}{\partial X^2}=\beta^2\tilde{\mathcal{L}}_1(\bar{W}_0,\bar{F}_{7/2})\\ +\beta^2\tilde{\mathcal{L}}_1(\bar{W}_{1/2},\bar{F}_3)+\beta^2\tilde{\mathcal{L}}_1(\bar{W}_1,\bar{F}_{5/2})+\beta^2\tilde{\mathcal{L}}_1(\bar{W}_{3/2},\bar{F}_2)\\ \quad+\beta^2\tilde{\mathcal{L}}_1(\bar{W}_2+W^*,\bar{F}_{3/2})\\ +\beta^2\tilde{\mathcal{L}}_1(\bar{W}_{5/2},\bar{F}_1)+\beta^2\tilde{\mathcal{L}}_1(\bar{W}_3,\bar{F}_{1/2})+\beta^2\tilde{\mathcal{L}}_1(\bar{W}_{7/2},\bar{F}_0)\\ \mathcal{L}_{21}(\bar{F}_{7/2})+2\bar{\tau}\mathcal{L}_{22}(\bar{W}_{7/2})+\frac{\partial^2\bar{W}_{7/2}}{\partial X^2}=-\frac{\beta^2}{2}\tilde{\mathcal{L}}_1(\bar{W}_0,\bar{W}_{7/2})\\ \quad-\frac{\beta^2}{2}\tilde{\mathcal{L}}_1(\bar{W}_{1/2},\bar{W}_3)-\frac{\beta^2}{2}\tilde{\mathcal{L}}_1(\bar{W}_1,\bar{W}_{5/2})\\ -\frac{\beta^2}{2}\tilde{\mathcal{L}}_1(\bar{W}_{3/2},\bar{W}_2+2W^*)-\bar{\tau}\vartheta_1\beta^2\tilde{\mathcal{L}}_2(\bar{W}_0,\bar{W}_{7/2})\\ \quad-\bar{\tau}\vartheta_1\beta^2\tilde{\mathcal{L}}_2(\bar{W}_{1/2},\bar{W}_3)\\ -\bar{\tau}\vartheta_1\beta^2\tilde{\mathcal{L}}_2(\bar{W}_1,\bar{W}_{5/2})-\bar{\tau}\vartheta_1\beta^2\tilde{\mathcal{L}}_2(\bar{W}_{3/2},\bar{W}_2+2W^*)\\ \quad+\bar{\tau}\vartheta_2\tilde{\mathcal{L}}_3(\bar{W}_0,\bar{W}_{7/2})\\ +\bar{\tau}\vartheta_2\tilde{\mathcal{L}}_3(\bar{W}_{1/2},\bar{W}_3)+\bar{\tau}\vartheta_2\tilde{\mathcal{L}}_3(\bar{W}_1,\bar{W}_{5/2})\\ \quad+\bar{\tau}\vartheta_2\tilde{\mathcal{L}}_3(\bar{W}_{3/2},\bar{W}_2+2W^*)+\frac{\bar{\tau}\vartheta_3\beta^2}{2}\tilde{\mathcal{L}}_4(\bar{W}_0,\bar{W}_{7/2})\\ +\frac{\bar{\tau}\vartheta_3\beta^2}{2}\tilde{\mathcal{L}}_4(\bar{W}_{1/2},\bar{W}_3)+\frac{\bar{\tau}\vartheta_3\beta^2}{2}\tilde{\mathcal{L}}_4(\bar{W}_1,\bar{W}_{5/2})\\ \quad+\frac{\bar{\tau}\vartheta_3\beta^2}{2}\tilde{\mathcal{L}}_4(\bar{W}_{3/2},\bar{W}_2+2W^*)\\ \mathcal{L}_{31}(\bar{W}_{5/2})+\mathcal{L}_{32}(\bar{\Psi}_{x_{7/2}})+\vartheta_5\beta\frac{\partial^2\bar{\Psi}_{y_{7/2}}}{\partial X\partial Y}=0\\ \mathcal{L}_{41}(\bar{W}_{5/2})+\mathcal{L}_{42}(\bar{\Psi}_{y_{7/2}})+\vartheta_5\beta\frac{\partial^2\bar{\Psi}_{x_{7/2}}}{\partial X\partial Y}=0\end{cases}$$

$$O(\epsilon^4):\begin{cases}\mathcal{L}_{11}(\bar{W}_2)+2\bar{\tau}\mathcal{L}_{12}(\bar{W}_2)+\mathcal{L}_{13}(\bar{\Psi}_{x_3})+\mathcal{L}_{14}(\bar{\Psi}_{y_3})-\frac{\partial^2\bar{F}_4}{\partial X^2}\\ \quad=\beta^2\tilde{\mathcal{L}}_1(\bar{W}_0,\bar{F}_4)+\beta^2\tilde{\mathcal{L}}_1(\bar{W}_{1/2},\bar{F}_{7/2})\\ +\beta^2\tilde{\mathcal{L}}_1(\bar{W}_1,\bar{F}_3)+\beta^2\tilde{\mathcal{L}}_1(\bar{W}_{3/2},\bar{F}_{5/2})+\beta^2\tilde{\mathcal{L}}_1(\bar{W}_2+W^*,\bar{F}_2)\\ \quad+\beta^2\tilde{\mathcal{L}}_1(\bar{W}_{5/2},\bar{F}_{3/2})\\ +\beta^2\tilde{\mathcal{L}}_1(\bar{W}_3,\bar{F}_1)+\beta^2\tilde{\mathcal{L}}_1(\bar{W}_{7/2},\bar{F}_{1/2})+\beta^2\tilde{\mathcal{L}}_1(\bar{W}_4,\bar{F}_0)+\mathcal{Q}_4\\ \mathcal{L}_{21}(\bar{F}_4)+2\bar{\tau}\mathcal{L}_{22}(\bar{W}_4)+\frac{\partial^2\bar{W}_4}{\partial X^2}=-\frac{\beta^2}{2}\tilde{\mathcal{L}}_1(\bar{W}_0,\bar{W}_4)\\ \quad-\frac{\beta^2}{2}\tilde{\mathcal{L}}_1(\bar{W}_{1/2},\bar{W}_{7/2})-\frac{\beta^2}{2}\tilde{\mathcal{L}}_1(\bar{W}_1,\bar{W}_3)\\ -\frac{\beta^2}{2}\tilde{\mathcal{L}}_1(\bar{W}_{3/2},\bar{W}_{5/2})-\frac{\beta^2}{2}\tilde{\mathcal{L}}_1(\bar{W}_2,\bar{W}_2+2W^*)\\ \quad-\bar{\tau}\vartheta_1\beta^2\tilde{\mathcal{L}}_2(\bar{W}_0,\bar{W}_4)\\ -\bar{\tau}\vartheta_1\beta^2\tilde{\mathcal{L}}_2(\bar{W}_{1/2},\bar{W}_{7/2})-\bar{\tau}\vartheta_1\beta^2\tilde{\mathcal{L}}_2(\bar{W}_1,\bar{W}_3)\\ \quad-\bar{\tau}\vartheta_1\beta^2\tilde{\mathcal{L}}_2(\bar{W}_{3/2},\bar{W}_{5/2})\\ -\bar{\tau}\vartheta_1\beta^2\tilde{\mathcal{L}}_2(\bar{W}_2,\bar{W}_2+2W^*)+\bar{\tau}\vartheta_2\tilde{\mathcal{L}}_3(\bar{W}_0,\bar{W}_4)\\ \quad+\bar{\tau}\vartheta_2\tilde{\mathcal{L}}_3(\bar{W}_{1/2},\bar{W}_{7/2})+\bar{\tau}\vartheta_2\tilde{\mathcal{L}}_3(\bar{W}_1,\bar{W}_3)\\ +\bar{\tau}\vartheta_2\tilde{\mathcal{L}}_3(\bar{W}_{3/2},\bar{W}_{5/2})+\bar{\tau}\vartheta_2\tilde{\mathcal{L}}_3(\bar{W}_2,\bar{W}_2+2W^*)\\ \quad+\frac{\bar{\tau}\vartheta_3\beta^2}{2}\tilde{\mathcal{L}}_4(\bar{W}_0,\bar{W}_4)\\ +\frac{\bar{\tau}\vartheta_3\beta^2}{2}\tilde{\mathcal{L}}_4(\bar{W}_{1/2},\bar{W}_{7/2})+\frac{\bar{\tau}\vartheta_3\beta^2}{2}\tilde{\mathcal{L}}_4(\bar{W}_1,\bar{W}_3)\\ \quad+\frac{\bar{\tau}\vartheta_3\beta^2}{2}\tilde{\mathcal{L}}_4(\bar{W}_{3/2},\bar{W}_{5/2})\\ +\frac{\bar{\tau}\vartheta_3\beta^2}{2}\tilde{\mathcal{L}}_4(\bar{W}_2,\bar{W}_2+2W^*)\\ \mathcal{L}_{31}(\bar{W}_3)+\mathcal{L}_{32}(\bar{\Psi}_{x_4})+\vartheta_5\beta\frac{\partial^2\bar{\Psi}_{y_4}}{\partial X\partial Y}=0\\ \mathcal{L}_{41}(\bar{W}_3)+\mathcal{L}_{42}(\bar{\Psi}_{y_4})+\vartheta_5\beta\frac{\partial^2\bar{\Psi}_{x_4}}{\partial X\partial Y}=0\end{cases}\tag{A1}$$

The sets of perturbation equations for the boundary layer solutions are:

$$O(\epsilon^{5/2}):\begin{cases}-e_{11}^*\frac{\partial^4\tilde{W}_{3/2}}{\partial\xi^4}-d_{11}^*\frac{\partial^3\tilde{\Psi}_{x_2}}{\partial\xi^3}-\frac{\partial^2\tilde{F}_{5/2}}{\partial\xi^2}=0\\ \vartheta_1\frac{\partial^4\tilde{F}_{5/2}}{\partial\xi^4}+(1-2\bar{\tau}\vartheta_1)\frac{\partial^2\tilde{W}_{3/2}}{\partial\xi^2}=0\\ -k_s a_{55}^*\frac{\partial\tilde{W}_{3/2}}{\partial\xi}-k_s a_{55}\tilde{\Psi}_{x_2}=0\\ -k_s a_{55}^*\tilde{\Psi}_{y_{5/2}}=0\end{cases}$$

$$O(\epsilon^3):\begin{cases}-e_{11}^*\frac{\partial^4\tilde{W}_2}{\partial\xi^4}-d_{11}^*\frac{\partial^3\tilde{\Psi}_{x_{5/2}}}{\partial\xi^3}-\frac{\partial^2\tilde{F}_3}{\partial\xi^2}=0\\ \vartheta_1\frac{\partial^4\tilde{F}_3}{\partial\xi^4}+(1-2\bar{\tau}\vartheta_1)\frac{\partial^2\tilde{W}_2}{\partial\xi^2}=0\\ -k_s a_{55}^*\frac{\partial\tilde{W}_2}{\partial\xi}-k_s a_{55}\tilde{\Psi}_{x_{5/2}}=0\\ -k_s a_{55}^*\tilde{\Psi}_{y_3}=0\end{cases}$$

$$O(\epsilon^3):\begin{cases}-e_{11}^*\frac{\partial^4\tilde{W}_2}{\partial\xi^4}-d_{11}^*\frac{\partial^3\tilde{\Psi}_{x_{5/2}}}{\partial\xi^3}-\frac{\partial^2\tilde{F}_3}{\partial\xi^2}=0\\ \vartheta_1\frac{\partial^4\tilde{F}_3}{\partial\xi^4}+(1-2\bar{\tau}\vartheta_1)\frac{\partial^2\tilde{W}_2}{\partial\xi^2}=0\\ -k_s a_{55}^*\frac{\partial\tilde{W}_2}{\partial\xi}-k_s a_{55}\tilde{\Psi}_{x_{5/2}}=0\\ -k_s a_{55}^*\tilde{\Psi}_{y_3}=0\end{cases}$$

$$O(\epsilon^{5/2}):\begin{cases}-e_{11}^*\frac{\partial^4\hat{W}_{3/2}}{\partial\varsigma^4}+d_{11}^*\frac{\partial^3\hat{\Psi}_{x_2}}{\partial\varsigma^3}-\frac{\partial^2\hat{F}_{5/2}}{\partial\varsigma^2}=0\\ \vartheta_1\frac{\partial^4\hat{F}_{5/2}}{\partial\varsigma^4}+(1-2\bar{\tau}\vartheta_1)\frac{\partial^2\hat{W}_{3/2}}{\partial\varsigma^2}=0\\ k_s a_{55}^*\frac{\partial\hat{W}_{3/2}}{\partial\varsigma}-k_s a_{55}\hat{\Psi}_{x_2}=0\\ -k_s a_{55}^*\hat{\Psi}_{y_{5/2}}=0\end{cases}$$

$$O(\epsilon^3):\begin{cases}-e_{11}^*\frac{\partial^4\hat{W}_2}{\partial\varsigma^4}+d_{11}^*\frac{\partial^3\hat{\Psi}_{x_{5/2}}}{\partial\varsigma^3}-\frac{\partial^2\hat{F}_3}{\partial\varsigma^2}=0\\ \vartheta_1\frac{\partial^4\hat{F}_3}{\partial\varsigma^4}+(1-2\bar{\tau}\vartheta_1)\frac{\partial^2\hat{W}_2}{\partial\varsigma^2}=0\\ k_s a_{55}^*\frac{\partial\hat{W}_2}{\partial\varsigma}-k_s a_{55}\hat{\Psi}_{x_{5/2}}=0\\ -k_s a_{55}^*\hat{\Psi}_{y_3}=0\end{cases}\tag{A2}$$

The obtained asymptotic solutions corresponding to clamped edge supports are:

$$\begin{aligned}W=&\mathcal{A}_{00}^{(0)}+\epsilon^{3/2}\Big[\mathcal{A}_{00}^{(3/2)}-\mathcal{A}_{00}^{(3/2)}\Big(\sin\Big(\frac{\alpha X}{\sqrt{\epsilon}}\Big)+\cos\Big(\frac{\alpha X}{\sqrt{\epsilon}}\Big)\Big)e^{-\frac{\alpha X}{\sqrt{\epsilon}}}\\ &-\mathcal{A}_{00}^{(3/2)}\Big(\sin\Big(\frac{\alpha(\pi-X)}{\sqrt{\epsilon}}\Big)+\cos\Big(\frac{\alpha(\pi-X)}{\sqrt{\epsilon}}\Big)\Big)e^{-\frac{\alpha(\pi-X)}{\sqrt{\epsilon}}}\Big]\\ &+\epsilon^2\Big[\mathcal{A}_{00}^{(2)}+\mathcal{A}_{11}^{(2)}\sin(mX)\sin(nY)-\mathcal{A}_{00}^{(2)}(\sin\Big(\frac{\alpha X}{\sqrt{\epsilon}}\Big)\\ &+\cos\Big(\frac{\alpha X}{\sqrt{\epsilon}}\Big))e^{-\frac{\alpha X}{\sqrt{\epsilon}}}-\mathcal{A}_{00}^{(2)}(\sin\Big(\frac{\alpha(\pi-X)}{\sqrt{\epsilon}}\Big)\\ &+\cos\Big(\frac{\alpha(\pi-X)}{\sqrt{\epsilon}}\Big))e^{-\frac{\alpha(\pi-X)}{\sqrt{\epsilon}}}\Big]\\ &+\epsilon^4\Big[\mathcal{A}_{00}^{(4)}+\mathcal{A}_{11}^{(4)}\sin(mX)\sin(nY)+\mathcal{A}_{20}^{(4)}\cos(2mX)\\ &+\mathcal{A}_{22}^{(4)}\cos(2mX)\cos(2nY)\Big]+O(\epsilon^5)\end{aligned}\tag{A3}$$

$$\begin{aligned}F=&-\mathcal{B}_{00}^{(0)}\Big(\beta^2X^2+\frac{Y^2}{2}\Big)+\epsilon^2\Big[-\mathcal{B}_{00}^{(2)}\Big(\beta^2X^2+\frac{Y^2}{2}\Big)\\ &+\mathcal{B}_{11}^{(2)}\sin(mX)\sin(nY)\Big]\\ &+\epsilon^{5/2}[+\mathcal{A}_{00}^{(3/2)}\Big(b_{10}^{(3/2)}\sin\Big(\frac{\alpha X}{\sqrt{\epsilon}}\Big)+b_{01}^{(3/2)}\cos\Big(\frac{\alpha X}{\sqrt{\epsilon}}\Big)\Big)e^{-\frac{\alpha X}{\sqrt{\epsilon}}}\\ &+\mathcal{A}_{00}^{(3/2)}(b_{10}^{(5/2)}\sin\Big(\frac{\alpha(\pi-X)}{\sqrt{\epsilon}}\Big)+b_{01}^{(5/2)}\cos\Big(\frac{\alpha(\pi-X)}{\sqrt{\epsilon}}\Big))e^{-\frac{\alpha(\pi-X)}{\sqrt{\epsilon}}}]\\ &+\epsilon^3\Big[\mathcal{A}_{00}^{(2)}\Big(b_{10}^{(3)}\sin\Big(\frac{\alpha X}{\sqrt{\epsilon}}\Big)+b_{01}^{(3)}\cos\Big(\frac{\alpha X}{\sqrt{\epsilon}}\Big)\Big)e^{-\frac{\alpha X}{\sqrt{\epsilon}}}\\ &+\mathcal{A}_{00}^{(2)}\Big(b_{10}^{(3)}\sin\Big(\frac{\alpha(\pi-X)}{\sqrt{\epsilon}}\Big)+b_{01}^{(3)}\cos\Big(\frac{\alpha(\pi-X)}{\sqrt{\epsilon}}\Big)\Big)e^{-\frac{\alpha(\pi-X)}{\sqrt{\epsilon}}}\Big]\\ &+\epsilon^4\Big[-\mathcal{B}_{00}^{(4)}\Big(\beta^2X^2+\frac{Y^2}{2}\Big)+\mathcal{B}_{20}^{(4)}\cos(2mX)+\mathcal{B}_{02}^{(4)}\cos(2mY)\\ &+\mathcal{B}_{22}^{(4)}\cos(2mX)\cos(2nY)\Big]+O(\epsilon^5)\end{aligned}\tag{A4}$$

$$\begin{aligned}\Psi_x=&\epsilon^2\Big[\Big(c_{10}^{(2)}\sin\Big(\frac{\alpha X}{\sqrt{\epsilon}}\Big)+c_{01}^{(2)}\cos\Big(\frac{\alpha X}{\sqrt{\epsilon}}\Big)\Big)e^{-\frac{\alpha X}{\sqrt{\epsilon}}}\\ &+\Big(c_{10}^{(2)}\sin\Big(\frac{\alpha(\pi-X)}{\sqrt{\epsilon}}\Big)+c_{01}^{(2)}\cos\Big(\frac{\alpha(\pi-X)}{\sqrt{\epsilon}}\Big)\Big)e^{-\frac{\alpha(\pi-X)}{\sqrt{\epsilon}}}\Big]\\ &+\epsilon^3[\mathcal{C}_{11}^{(3)}\cos(mX)\sin(nY)]+O(\epsilon^5)\end{aligned}\tag{A5}$$

$$\Psi_y=\epsilon^3[\mathcal{D}_{11}^{(3)}\sin(mX)\cos(nY)]++O(\epsilon^5)\tag{A6}$$

$$\mathcal{A}_{00}^{(0)}=0\tag{A7}$$

The periodicity condition yields

$$\mathcal{A}_{00}^{(3/2)}=\frac{2}{3}3^{1/4}\mathcal{P}_q\Big(\frac{2\vartheta_1-\vartheta_2}{1-2\bar{\tau}\vartheta_1}\Big)+\frac{2\bar{\tau}\vartheta_6(\vartheta_1-\vartheta_2)}{1-2\bar{\tau}\vartheta_1}\epsilon^{-1/2}\tag{A8}$$

$$\mathcal{A}_{00}^{(2)}=\mathcal{A}_{00}^{(3)}=0\tag{A9}$$

$$\mathcal{A}_{00}^{(4)}=\frac{2\bar{\tau}\vartheta_2m^2+\beta^2n^2(1-2\bar{\tau}\vartheta_1)(1+2\ell)}{8(1-2\bar{\tau}\vartheta_1)}(\mathcal{A}_{11}^{(2)})^2\tag{A10}$$

The parameters in equations (37-40) are as follows

$$\mathcal{P}_q^{(0)}=K_0K_1+\epsilon^2\beta^2K_4\tag{A11}$$

$$\mathcal{P}_q^{(2)} = 8K_1K_9K_{14} + \frac{8K_1K_9(K_0K_1K_{13}\beta^2 + K_0K_9K_{12})}{K_0K_1\beta^2 - K_{12}} + \frac{4K_1K_9(K_0K_{13} + K_0^2K_9)}{K_0K_1\beta^2 - K_{12}} + 16K_0K_9K_{10} + \frac{4K_0K_1K_9K_{16}}{K_0K_{11} + K_{15}} \quad \text{(A12)}$$

$$\delta_q^{(0)} = \left[\frac{3^{3/4}}{2}\bar{\tau}\vartheta_6(\vartheta_1 - \vartheta_2)\right]\epsilon^{-1/2} + \frac{\bar{\tau}\vartheta_2\vartheta_6(\vartheta_1 - \vartheta_2)}{\pi\alpha\vartheta_1(1 - 2\bar{\tau}\vartheta_1)} + \left[\frac{\vartheta_1}{2} - \vartheta_2 - \bar{\tau}\vartheta_2\left(\frac{2\vartheta_1 - \vartheta_2}{1 - 2\bar{\tau}\vartheta_1}\right) + \left(\frac{2\vartheta_1\vartheta_2 - \vartheta_2^2}{\pi\alpha\vartheta_1}\right)\epsilon^{1/2}\right] \mathcal{P}_q + \left[\left(\frac{3^{1/4}\alpha(2\vartheta_1 - \vartheta_2)^2}{6\pi}\right)\epsilon\right]\mathcal{P}_q^2 \quad \text{(A13)}$$

$$\delta_q^{(2)} = \left[\frac{3^{3/4}}{32}(m^2(1 - 2\bar{\tau}\vartheta_1) + 2\bar{\tau}\vartheta_2\beta^2n^2)\right]\epsilon^{-3/2} \quad \text{(A14)}$$

where K_i (i = 0,..., 17) are the parameters in terms of ϑ_1, ϑ_2, ϑ_3, ϑ_4, ϑ_5, ℓ, m, n, β obtained via the sets of perturbation equations.

$$\mathcal{S}_1 = -\left[\left(\frac{2\vartheta_1 - \vartheta_2}{1 - 2\bar{\tau}\vartheta_1}\right)(\mathcal{P}_q^{(2)})\right] \quad \text{(A15)}$$

$$\mathcal{S}_2 = -\left(\frac{2\vartheta_1 - \vartheta_2}{1 - 2\bar{\tau}\vartheta_1}\right)(\mathcal{P}_q^{(0)}) - \frac{2\bar{\tau}\vartheta_6(\vartheta_1 - \vartheta_2)}{1 - 2\bar{\tau}\vartheta_1}\epsilon \quad \text{(A16)}$$

REFERENCES

[1] X. Li, B. Bhushan, K. Takashima, C.W. Baek, Y.K. Kim, Mechanical characterization of micro/nanoscale structures for MEMS/NEMS applications using nanoindentation techniques, Ultramicroscopy 97 (2003) 481–494.

[2] Y. Moser, M.A.M. Gijs, Miniaturized flexible temperature sensor, Journal of Microelectromechanics Systems 16 (2007) 1349–1354.

[3] K. Ahmad, W. Pan, Dramatic effect of multiwalled carbon nanotubes on the electrical properties of alumina based ceramic nanocomposites, Composites Science and Technology 69 (2009) 1016–1021.

[4] X. Yao, Q. Han, Torsional buckling and postbuckling equilibrium path of double-walled carbon nanotubes, Composites Science and Technology 68 (2008) 113–120.

[5] Y.G. Hu, K.M. Liew, Q. Wang, X.Q. He, B.I. Yakobson, Nonlocal shell model for elastic wave propagation in single- and double-walled carbon nanotubes, Journal of the Mechanics and Physics of Solids 56 (2008) 3475–3485.

[6] H.-S. Shen, C.L. Zhang, Torsional buckling and postbuckling of double-walled carbon nanotubes by nonlocal shear deformable shell model, Composite Structures 92 (2010) 1073–1084.

[7] B. Wang, J. Zhao, Sh. Zhou, A micro scale Timoshenko beam model based on strain gradient elasticity theory, European Journal of Mechanics – A/Solids 29 (2010) 591–599.

[8] W. Xia, L. Wang, L. Yin, Nonlinear non-classical microscale beams: Static bending, postbuckling and free vibration, International Journal of Engineering Science 48 (2010) 2044–2053.

[9] R. Ansari, S. Sahmani, B. Arash, Nonlocal plate model for free vibrations of single-layered graphene sheets, Physics Letters A 375 (2010) 53–62.

[10] R. Ansari, S. Sahmani, H. Rouhi, Axial buckling analysis of single-walled carbon nanotubes in thermal environments via Rayleigh-Ritz technique, Computational Materials Science 50 (2011) 3050–3055.

[11] R. Ansari, R. Gholami, S. Sahmani, Free vibration analysis of size-dependent functionally graded microbeams based on the strain gradient Timoshenko beam theory, Composite Structures 94 (2011) 221–228.

[12] R. Ansari, S. Sahmani, Small scale effect on vibrational response of single-walled carbon nanotubes with different boundary conditions based on nonlocal beam models, Communications in Nonlinear Science and Numerical Simulation 17 (2012) 1965–1979.

[13] R. Ansari, S. Sahmani, Prediction of biaxial buckling behavior of single-layered graphene sheets based on nonlocal plate models and molecular dynamics simulations, Applied Mathematical Modelling 37 (2013) 7338–7351.

[14] S. Sahmani, R. Ansari, Size-dependent buckling analysis of functionally graded third-order shear deformable microbeams including thermal environment effect, Applied Mathematical Modelling 37 (2013) 9499–9515.

[15] S. Sahmani, R. Ansari, On the free vibration response of functionally graded higher-order shear deformable microplates based on the strain gradient elasticity theory, Composite Structures 95 (2013) 430–442.

[16] S. Sahmani, R. Ansari, R. Gholami, A. Darvizeh, Dynamic stability analysis of functionally graded higher-order shear deformable microshells based on the modified couple stress elasticity theory, Composites Part B: Engineering 51 (2013) 44–53.

[17] H.-S. Shen, Nonlocal shear deformable shell model for torsional buckling and postbuckling of microtubules in thermal environment, Mechanics Research Communications 54 (2013) 83–95.

[18] A.K. Lazopoulos, K.A. Lazopoulos, G. Palassopoulos, Nonlinear bending and buckling for strain gradient elastic beams, Applied Mathematical Modelling 38 (2014) 253–262.

[19] S. Sahmani, M. Bahrami, R. Ansari, Nonlinear free vibration analysis of functionally graded third-order shear deformable microbeams based on the modified strain gradient elasticity theory, Composite Structures 110 (2014) 219–230.

[20] B. Akgöz, Ö. Civalek, Thermo-mechanical buckling behavior of functionally graded microbeams embedded in elastic medium, International Journal of Engineering Science 85 (2014) 90–104.

[21] Y.S. Li, Z.Y. Cai, S.Y. Shi, Buckling and free vibration of magnetoelectroelastic nanoplate based on nonlocal theory, Composite Structures 111 (2014) 522–529.

[22] Y.-G. Wang, W.-H. Lin, N. Liu, Nonlinear bending and post-buckling of extensible microscale beams based on modified couple stress theory, Applied Mathematical Modelling 39 (2015) 117–127.

[23] H.L. Dai, L. Wang, A. Abdelkefi, Q. Ni, On nonlinear behavior and buckling of fluid-transporting nanotubes, International Journal of Engineering Science 87 (2015) 13–22.

[24] M.E. Gurtin, A.I. Murdoch, A continuum theory of elastic material surface, Archive for Rational Mechanics and Analysis 57 (1975) 291–323.

[25] M.E. Gurtin, A.I. Murdoch, Surface stress in solids, International Journal of Solids and Structures 14 (1978) 431–440.

[26] M.E. Gurtin, J. Weissmuller, F. Larche, A general theory of curved deformable interfaces in solids at equilibrium, Philos Magnetic A 78 (1998) 1093–1109.

[27] J. Weissmuller, J.W. Cahn, Mean stresses in microstructures due to interface stresses: A generalization of a capillary equation for solids, Acta Materialla 45 (1997) 1899–1906.

[28] H.L. Duan, J. Wang, Z.P. Huang, B.L. Karihaloo, Size-dependent effective elastic constants of solids containing nano-inhomogeneities with interface stress, Journal of Mechanics and Physics of Solids 53 (2005) 1574–1596.

[29] P. Sharma, S. Ganti, N. Bhate, Effect of surfaces on the size-dependent elastic state of nano-inhomogeneities, Applied Physics Letters 82 (2003) 535.
[30] P. Sharma, L.T. Wheeler, Size-dependent elastic state of ellipsoidal nano-inclusion incorporating surface/interface tension, ASME Journal of Applied Mechanics 74 (2007) 447–454.
[31] C.W. Lim, L.H. He, Size-dependent nonlinear response of thin elastic films with nano-scale thickness, International Journal of Mechanical Sciences 46 (2004) 1715–1726.
[32] Z.R. Li, C.W. Lim, L.H. He, Stress concentration around a nano-scale spherical cavity in elastic media: effect of surface stress, European Journal of Mechanics – A/Solids 25 (2006) 260–270.
[33] L. Tian, R.K.N.D. Rajapakse, Analytical solution for size-dependent elastic field of a nanoscale circular inhomogeneity, ASME Journal of Applied Mechanics 74 (2007) 568–574.
[34] L. Tian, R.K.N.D. Rajapakse, Elastic field of an isotropic matrix with a nanoscale elliptical inhomogeneity, International Journal of Solids and Structures 44 (2007) 7988–8005.
[35] C.F. Lu, W.Q. Chen, C.W. Lim, Elastic mechanical behavior of nano-scaled FGM films incorporating surface energies, Composites Science and Technology 69 (2009) 1124–1130.
[36] E. Gordeliy, S.G. Mogilevskaya, S.L. Crouch, Transient thermal stress in a medium with a circular cavity with surface effects, International Journal of Solids and Structures 46 (2009) 1834–1848.
[37] S.G. Mogilevskaya, S.L. Crouch, A.L. Grotta, H.K. Stolarski, The effects of surface elasticity and surface tension on the transverse overall elastic behavior of unidirectional nano-composites, Composites Science and Technology 70 (2010) 427–434.
[38] Y. Fu, J. Zhang, Y. Jiang, Influences of the surface energies on the nonlinear static and dynamic behaviors of nanobeams, Physica E 42 (2010) 2268–2273.
[39] R. Ansari, S. Sahmani, Bending behavior and buckling of nanobeams including surface stress effects corresponding to different beam theories, International Journal of Engineering Science 49 (2011) 1244–1255.
[40] R. Ansari, S. Sahmani, Surface stress effects on the free vibration behavior of nanoplates, International Journal of Engineering Science 49 (2011) 1204–1215.
[41] L. Wang, Surface effect on buckling configuration of nanobeams containing internal flowing fluid: A nonlinear analysis, Physica E 44 (2012) 808–812.
[42] R. Ansari, V. Mohammadi, M. Faghih Shojaei, R. Gholami, S. Sahmani, Postbuckling characteristics of nanobeams based on the surface elasticity theory, Composites Part B: Engineering 55 (2013) 240–246.
[43] R. Ansari, V. Mohammadi, M. Faghih Shojaei, R. Gholami, S. Sahmani, Postbuckling analysis of Timoshenko nanobeams including surface stress effect, International Journal of Engineering Science 75 (2014) 1–10.
[44] K. Kiani, Surface effect on free transverse vibrations and dynamic instability of current carrying nanowires in the presence of a longitudinal magnetic field, Physics Letters A 378 (2014) 1834–1840.
[45] F. Gao, Q. Cheng, J. Luo, Mechanics of nanowire buckling on elastomeric substrates with consideration of surface stress effects, Physica E 64 (2014) 72–77.
[46] R. Ansari, R. Gholami, M. Faghih Shojaei, V. Mohammadi, S. Sahmani, Surface stress effect on the pull-in instability of circular nanoplates, Acta Astronautica 102 (2014) 140–150.
[47] S. Sahmani, M. Bahrami, R. Ansari, Surface energy effects on the free vibration characteristics of postbuckled third-order shear deformable nanobeams, Composite Structures 116 (2014) 552–561.
[48] S. Sahmani, M. Bahrami, R. Ansari, Surface effects on the free vibration behavior of postbuckled circular higher-order shear deformable nanoplates including geometrical nonlinearity, Acta Astronautica 105 (2014) 417–427.
[49] S. Sahmani, M. Bahrami, M.M. Aghdam, R. Ansari, Surface effects on the nonlinear forced vibration response of third-order shear deformable nanobeams, Composite Structures 118 (2014) 149–158.
[50] X. Liang, S. Hu, S. Shen, Surface effects on the post-buckling of piezoelectric nanowires, Physica E 69 (2015) 61–64.
[51] S. Sahmani, M.M. Aghdam, M. Bahrami, On the free vibration characteristics of postbuckled third-order shear deformable FGM nanobeams including surface effects, Composite Structures 121 (2015) 377–385.
[52] S. Sahmani, M. Bahrami, M.M. Aghdam, R. Ansari, Postbuckling behavior of circular higher-order shear deformable nanoplates including surface energy effects, Applied Mathematical Modelling 39 (2015) 3678–3689.
[53] L.H. Donnell, Beam, plates and shells, McGraw-Hill, New York, USA, 1976, pp. 377–445.
[54] H.-S. Shen, Boundary layer theory for the buckling and postbuckling of an anisotropic laminated cylindrical shell. Part II: Prediction under external pressure, Composite Structures 82 (2008) 362–370.
[55] H.-S. Shen, Postbuckling of shear deformable FGM cylindrical shells surrounded by an elastic medium, International Journal of Mechanical Sciences 51 (2009) 372–383.
[56] H.-S. Shen, Postbuckling of nanotube-reinforced composite cylindrical shells in thermal environments, Part II: Pressure-loaded shells, Composite Structures 93 (2011) 2496–2503.
[57] H.-S. Shen, Postbuckling of functionally graded fiber reinforced composite laminated cylindrical shells, Part I: Theory and solutions, Composite Structures 94 (2012) 1305–1321.
[58] H.-S. Shen, Y. Xiang, Postbuckling of axially compressed nanotube-reinforced composite cylindrical panels resting on elastic foundations in thermal environments, Composites Part B: Engineering 67 (2014) 50–61.
[59] R.E. Miller, V.B. Shenoy, Size-dependent elastic properties of nanosized structural elements, Nanotechnology 11 (2000) 139–147.
[60] R. Zhu, E. Pan, P.W. Chung, X. Cai, K.M. Liew, A. Buldum, Atomistic calculation of elastic moduli in strained silicon, Semiconductor Science and Technology 21 (2006) 906–911.
[61] P. Mirfakhraei, D. Redekop, Buckling of circular cylindrical shells by the differential quadrature method, International Journal of Pressure Vessels and Piping 75 (1998) 347–353.